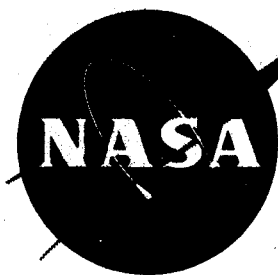


40p

554292

NASA TM X-211 4263

NASA TM X-211



N63-12915  
Code 1

# TECHNICAL MEMORANDUM

## X-211

THE AERODYNAMIC CHARACTERISTICS OF A BODY IN THE  
FLOW FIELD NEAR THE TIP OF A CIRCULAR-ARC  
WING OF RECTANGULAR PLAN FORM AT A

MACH NUMBER OF 2.01

By John P. Gapcynski

Langley Research Center  
Langley Field, Va.

Declassified February 6, 1962

NATIONAL AERONAUTICS AND SPACE ADMINISTRATION  
WASHINGTON

January 1960

NATIONAL AERONAUTICS AND SPACE ADMINISTRATION

TECHNICAL MEMORANDUM X-211

THE AERODYNAMIC CHARACTERISTICS OF A BODY IN THE  
FLOW FIELD NEAR THE TIP OF A CIRCULAR-ARC

WING OF RECTANGULAR PLAN FORM AT A

MACH NUMBER OF 2.01\*

By John P. Gapcynski

SUMMARY

An investigation has been conducted in the Langley 4- by 4-foot supersonic pressure tunnel to determine the aerodynamic characteristics of a body, with a fineness ratio of 8, in the three-dimensional flow field at the tip of an  $8\frac{1}{3}$ -percent-thick circular-arc wing of rectangular plan form. Force and pressure data on the body were obtained for several wing-body positions at a Mach number of 2.01 and a Reynolds number of  $3.4 \times 10^6$  per foot. Fairly good predictions of the trend and order of magnitude of the interference increments in the body forces and moments were obtained from an application of slender-body theory.

INTRODUCTION

An investigation has been conducted in the Langley 4- by 4-foot supersonic pressure tunnel to determine the characteristics of bodies and wings in flow fields with varying degrees of complexity. The first phase of this investigation was reported in reference 1, wherein the changes in the aerodynamic characteristics of a body were determined as the position of the body was varied with respect to a reflection plane aligned with the airstream. The second phase of this investigation (ref. 2) was concerned with the characteristics of a body in the two-dimensional flow field of a circular-arc wing of rectangular plan form. The effect of the body field on the wing was also considered although the analysis was not as extensive as that of the effect of the wing on the body.

---

\*Title, Unclassified.

Fairly good predictions of the trend and order of magnitude of the forces on the body due to these relatively simple flow fields were obtained with an application of slender-body theory.

In the present report the analysis of references 1 and 2 has been extended to the determination of the characteristics of a body in the three-dimensional flow field at the tip of the circular-arc, rectangular-plan-form wing used in reference 2. Pressure and force measurements on the body have been obtained for a range of chordwise, spanwise, and vertical (with respect to the chord plane) positions of the body with respect to the wing. Tests were made at a Mach number of 2.01 at a Reynolds number of  $3.4 \times 10^6$  per foot for a wing and body angle of attack of  $0^\circ$ . The data are compared with theoretical results obtained by an application of slender-body theory.

#### SYMBOLS

$\rho$	mass density of air
$V$	airspeed
$\alpha$	speed of sound in air
$M$	Mach number, $V/\alpha$
$q$	dynamic pressure, $\frac{1}{2}\rho V^2$
$p$	free-stream static pressure
$p_l$	local static pressure
$C_p$	pressure coefficient, $\frac{p_l - p}{q}$
$R$	local radius of body
$L$	length of body
$c$	wing chord length
$\theta$	body polar angle, deg (see fig. 1)
$x$	distance from apex of body measured along axis of symmetry

X	chordwise position of body nose with respect to wing midpoint, positive when measured upstream (see fig. 3)
Y	spanwise position of body center line with respect to wing tip, positive when body is inboard of tip (see fig. 3)
Z	vertical position of body nose with respect to wing chord plane (see fig. 3)
S	body cross-sectional area
$C_N$	body normal-force coefficient, positive towards wing, $\frac{\text{Body normal force}}{qS_{\max}}$
$C_m$	body pitching-moment coefficient about apex of body, $\frac{\text{Body pitching moment}}{qS_{\max}L}$
$\Delta C_D$	interference increment in body drag force, $\frac{\text{Body drag force increment}}{qS_{\max}}$
$C_Y$	body side-force coefficient, positive toward wing tip from a position inboard of the tip, $\frac{\text{Body side force}}{qS_{\max}}$
$C_n$	body yawing-moment coefficient about apex of body, $\frac{\text{Body yawing moment}}{qS_{\max}L}$

Subscript:

max          maximum

## DESCRIPTION OF MODELS AND TESTS

The model setup for the pressure tests is shown in figure 1. An  $8\frac{1}{3}$ -percent-thick circular-arc wing of rectangular plan form was mounted from the tunnel side wall on two sweptback struts. Chordwise and spanwise motion between the wing and the body was accomplished by movement of the wing along the tunnel side wall. Vertical motion between the

body and the wing (Z-direction) was obtained by translation of the body and the sting. In order to obtain a spanwise position of the body outboard of the tip, it was necessary to remove 2.25 inches of material from the tip of the wing.

The fuselage model was a blunt-based parabolic body of revolution with a length equal to that of the wing chord and with a fineness ratio of 8. The pressure model was equipped with two rows (located 180° apart) of static-pressure orifices, each row containing 24 orifices. Provision was made in the model sting for rolling the body about its own axis so that complete pressure coverage could be obtained.

The model setup for the force tests is shown in figure 2. The wing was mounted on a tunnel boundary-layer bypass plate. The body was sting mounted from the main tunnel support strut and housed a six-component strain-gage balance for the measurement of forces and moments. Vertical and spanwise motion of the body with respect to the wing was remotely controlled during each run. Axial or chordwise location was varied by changing the length of the support sting during shutdown between tunnel runs. Body base pressures were obtained by measurement of the balance cavity pressure and drag coefficients were corrected to free-stream conditions at the base.

Pressure and force measurements on the body were obtained for the wing-body positions shown on the test grid in figure 3. The small circles at the grid intersections identify the points at which data were obtained and signify the location of the body nose apex with respect to the wing-chord center line. The test Mach number was 2.01; the Reynolds number,  $3.4 \times 10^6$  per foot; and the wing and body angle of attack was 0°. Throughout the tests, transition strips (no. 60 carborundum grains) were installed on both the body and the wing.

Tunnel stagnation conditions were as follows: temperature, 110° F; dewpoint, approximately -35° F; and pressure, 14 pounds per square inch absolute.

## RESULTS AND DISCUSSION

### Presentation of Data

The basic-pressure data obtained on the body are presented in figure 4 as a function of body station and radial angle for each of the wing-body positions investigated. The zero reference for each radial angle position is indicated by the appropriate symbol at an  $x/L$  value

of zero. The data are presumed to be accurate to within  $\pm 0.01$  in pressure coefficient.

The variation of the body incremental drag, normal-force, side-force, pitching-moment, and yawing-moment coefficients with wing-body position are shown in figures 5, 6, 7, 8, and 9, respectively.

### Analysis

L One of the initial problems encountered in the determination of  
5 the characteristics of a body in a nonuniform flow field is the accurate  
3 definition of the field itself. This fact was pointed out in reference 2  
3 where it was noted that the wing flow field defined by linear theory did not appear to be an adequate representation of actual conditions.

This problem becomes more acute, of course, as the distance between the wing and body, and also, the thickness ratio of the wing are increased. For the two-dimensional flow of reference 2, both linear theory and the more accurate shock-expansion theory were used to obtain the field characteristics. Although no appreciable improvement in the total normal-force and pitching-moment variations was noted when the results obtained from shock-expansion theory were compared with those obtained from linear theory, there was a marked improvement in the predictions of body load distributions.

Unfortunately, there is no theory comparable to shock-expansion methods which is amenable to the calculation of the three-dimensional flow at the wing tip. Therefore, the results of this investigation were of necessity obtained with the use of a flow field defined by linear theory. Since the wing angle of attack was maintained at  $0^\circ$ , an additional restriction placed upon the analysis is that only wing-thickness effects are considered.

The predictions of the forces on the body in the wing flow field were determined from slender-body theory. This development is presented in the appendix of reference 2. Once the flow field itself has been determined, the body is superimposed in this field (with the assumption that the field is not disturbed in any manner) and the flow quantities along the body center line determine the interference forces on the body. An additional simplifying assumption which is made is that multiple reflections between the wing and body may be neglected. More accurate results may be obtained by a consideration of these reflections, but the applications are tedious and do not appear to be warranted.

### Body Force Characteristics

The spanwise variation of the force and moment increments on the body due to the interfering wing flow field are presented in figures 5 to 9 for each of the six chordwise and two vertical positions of the body with respect to the wing which were investigated. The sketches at the top of each figure serve to orient the data with respect to body position. The plain symbols represent data obtained from the force tests, and the solid symbols indicate the pressure test results. No pressure data are presented in these figures for X-values of -4 and -8 since the wing leading-edge shock was reflected from the tunnel wall back onto the body at these positions. The solid and dashed lines represent the estimation of these force and moment variations as obtained from slender-body theory.

The chord-force, normal-force, and pitching-moment variations appear to change smoothly through the tip region from free-stream conditions to the two-dimensional values indicated by the flagged solid symbols (from ref. 2) at the extreme right of each plot. (See figs. 5, 6, and 8.) Outboard of the tip the variation and magnitude of these quantities are small. Inboard of the tip the values rapidly approach two-dimensional conditions, the maximum drag increment experienced being equal to the body drag in undisturbed flow, and the maximum lift increment corresponding to the normal force experienced by this body at an angle of about  $8^\circ$ . The prediction of the trends and magnitudes of the chord-force, normal-force, and pitching-moment-coefficient variations are fairly representative of actual conditions although the estimation of specific values at any particular wing-body location may be subject to large error.

The spanwise variation of body side-force and yawing-moment coefficients (figs. 7 and 9, respectively) are fairly symmetrical about the wingtip except for the vertical position nearest the wing,  $Z = 1.5$ , and at the forward body chordwise locations. (For instance, note the sudden increase in side force on the body just inboard of the tip at  $X = 8$ .) The pressure and force results also do not agree in this region; this result may indicate that conditions may be changing very rapidly and small variations in body location may result in large changes in body forces. With the exception of these factors, the prediction of the side-force and yawing-moment coefficients is very good.

### CONCLUDING REMARKS

The changes in the aerodynamic characteristics of a blunt-based parabolic body of revolution with a fineness ratio of 8 have been

determined in the three-dimensional-flow field at the tip of an  $8\frac{1}{3}$ -percent-thick circular-arc wing of rectangular plan form. Both force and pressure data were obtained on the body at a Mach number of 2.01 and a Reynolds number of  $3.4 \times 10^6$  per foot, and the results have been compared with an application of slender-body theory. Fairly good predictions of the trend and order of magnitude of the interference increments in body drag, normal- and side-force coefficients, and body pitching- and yawing-moment coefficients were obtained.

Langley Research Center,  
National Aeronautics and Space Administration,  
Langley Field, Va., September 24, 1959.

#### REFERENCES

1. Gapcynski, John P., and Carlson, Harry W.: A Pressure-Distribution Investigation of the Aerodynamic Characteristics of a Body of Revolution in the Vicinity of a Reflection Plane at Mach Numbers of 1.41 and 2.01. NACA RM L54J29, 1955.
2. Gapcynski, John P., and Carlson, Harry W.: The Aerodynamic Characteristics of a Body in the Two-Dimensional Flow Field of a Circular-Arc Wing at a Mach Number of 2.01. NACA RM L57E14, 1957.

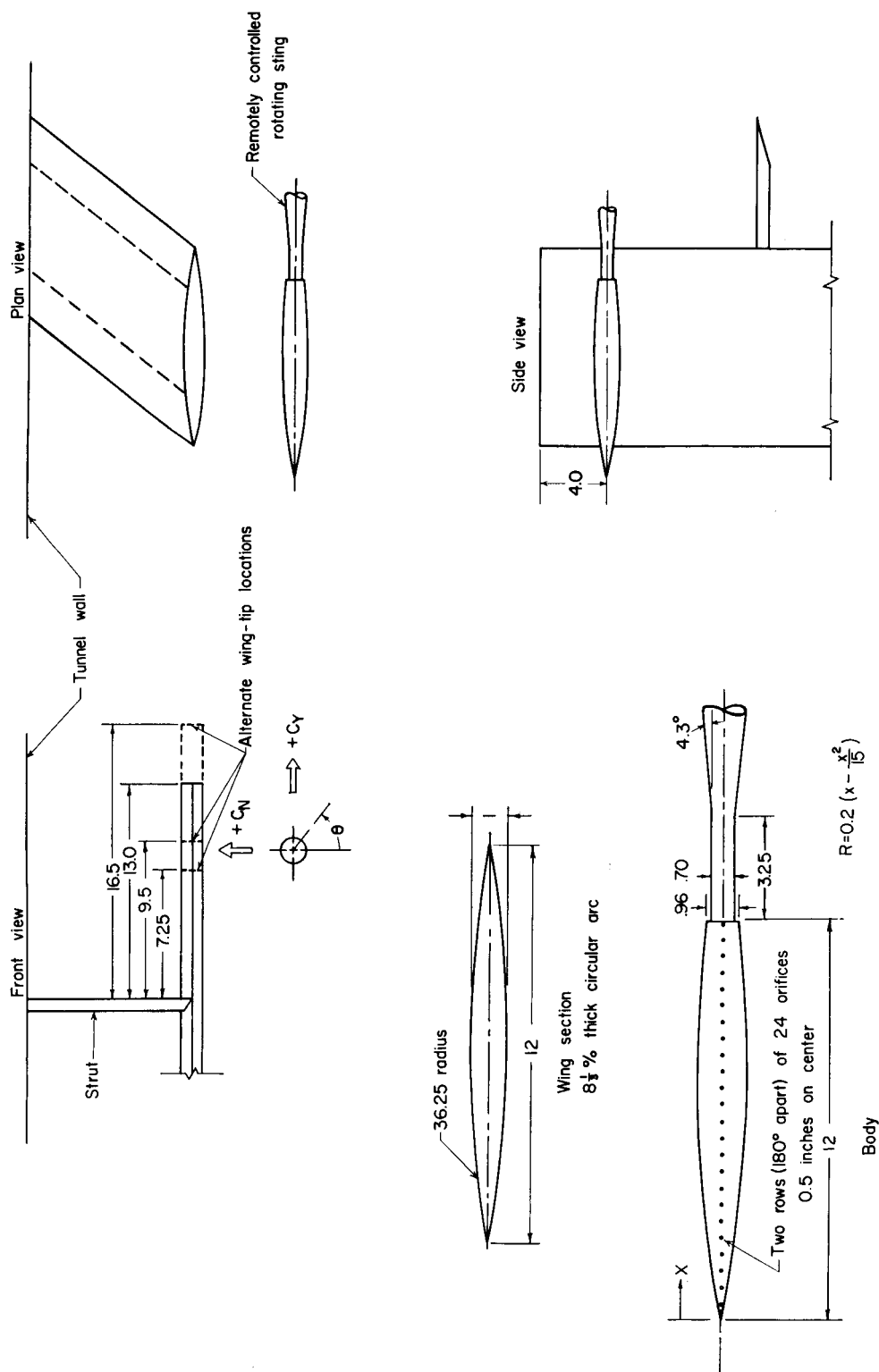


Figure 1.- Schematic layout of models and setup for pressure tests. All dimensions are in inches unless otherwise noted.

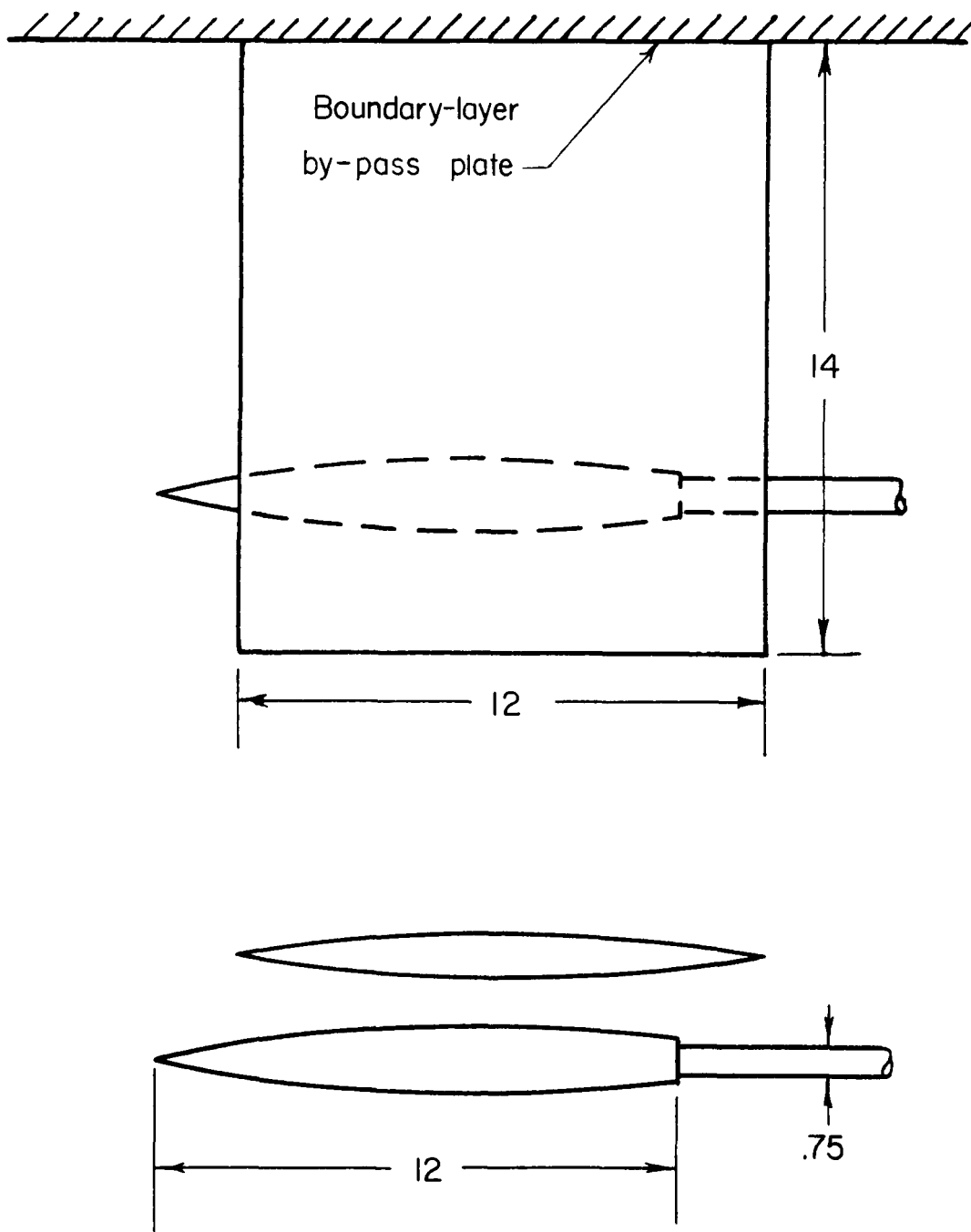
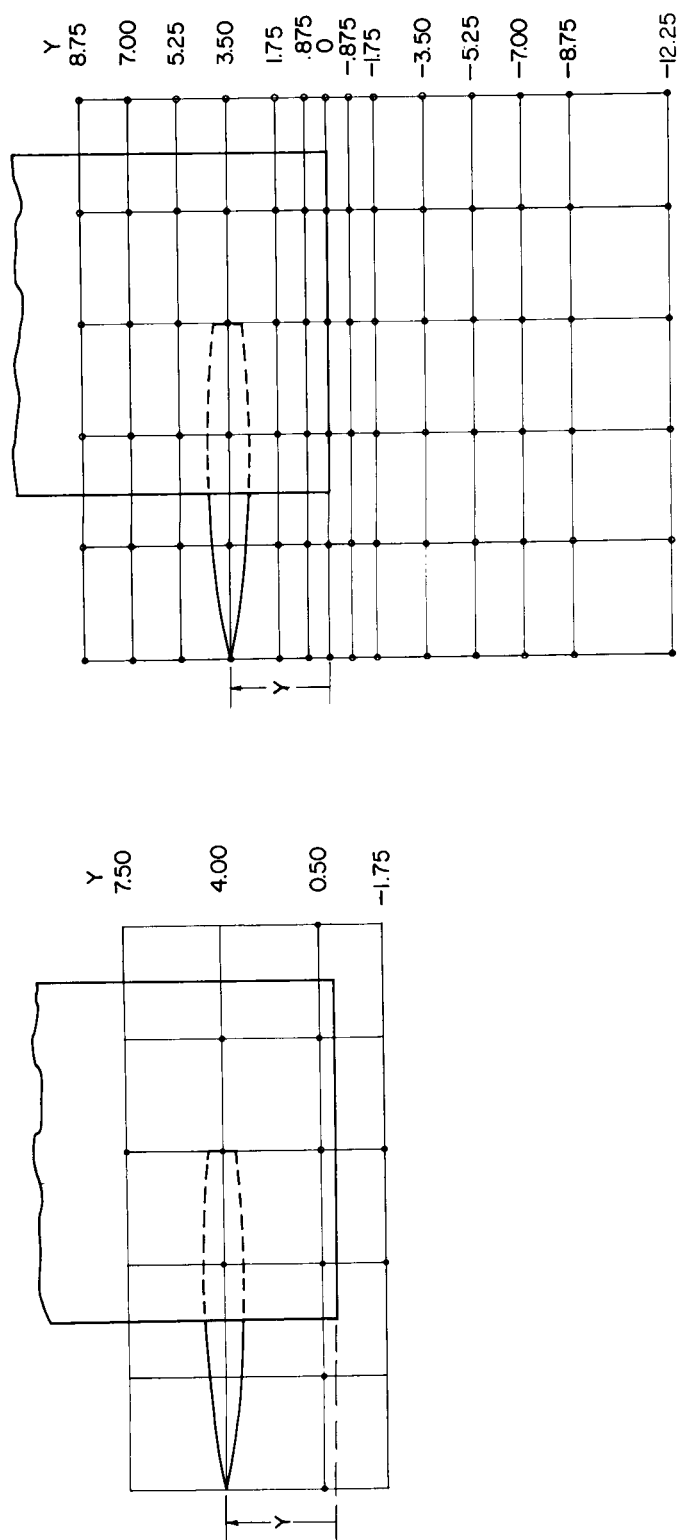
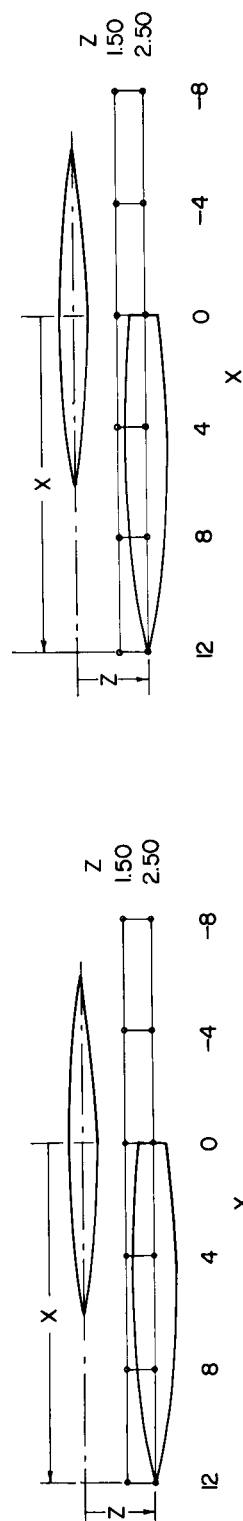


Figure 2.- Schematic layout of models and setup for force tests. All dimensions are in inches.

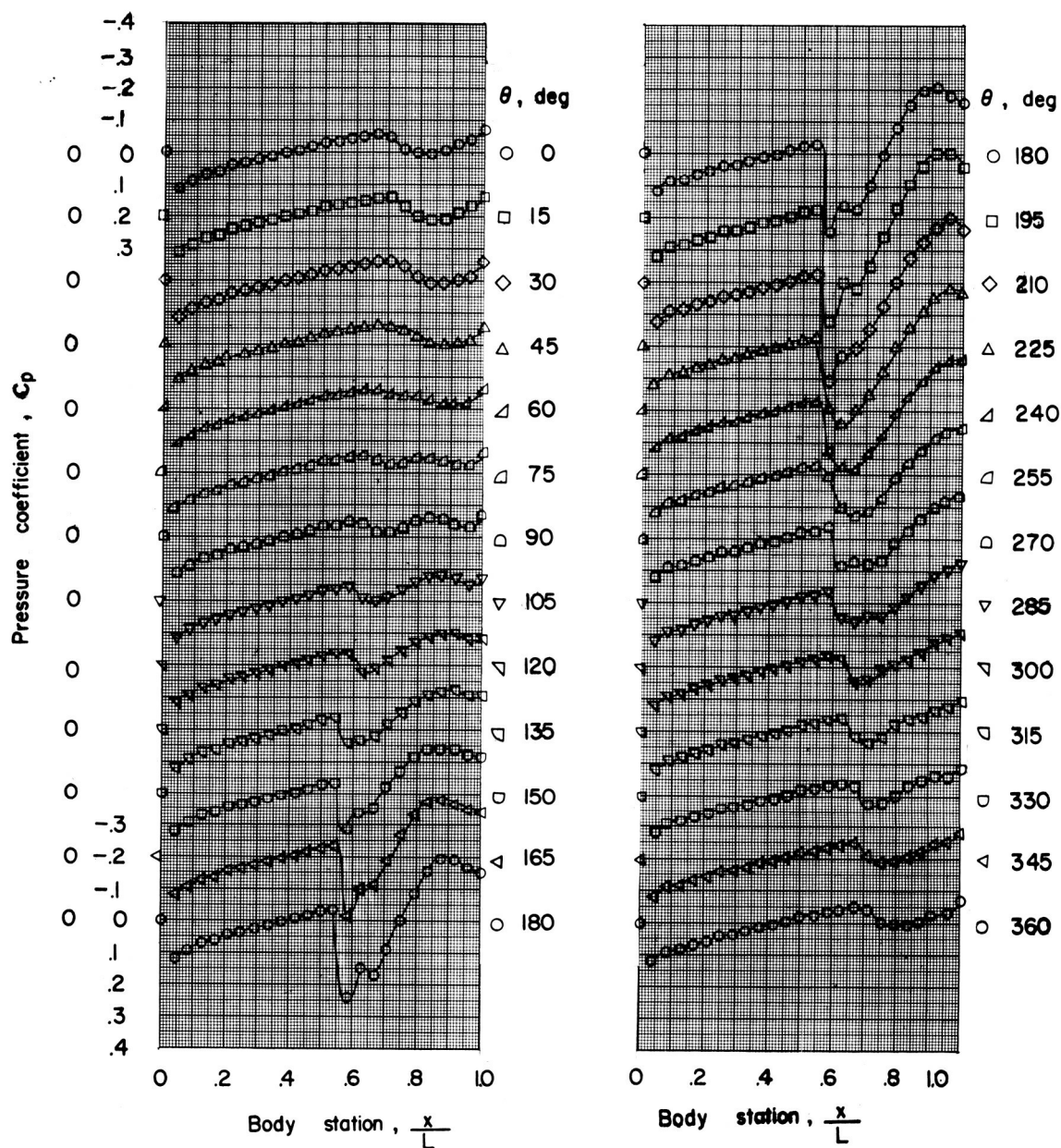


(a) Pressure tests.



(b) Force tests.

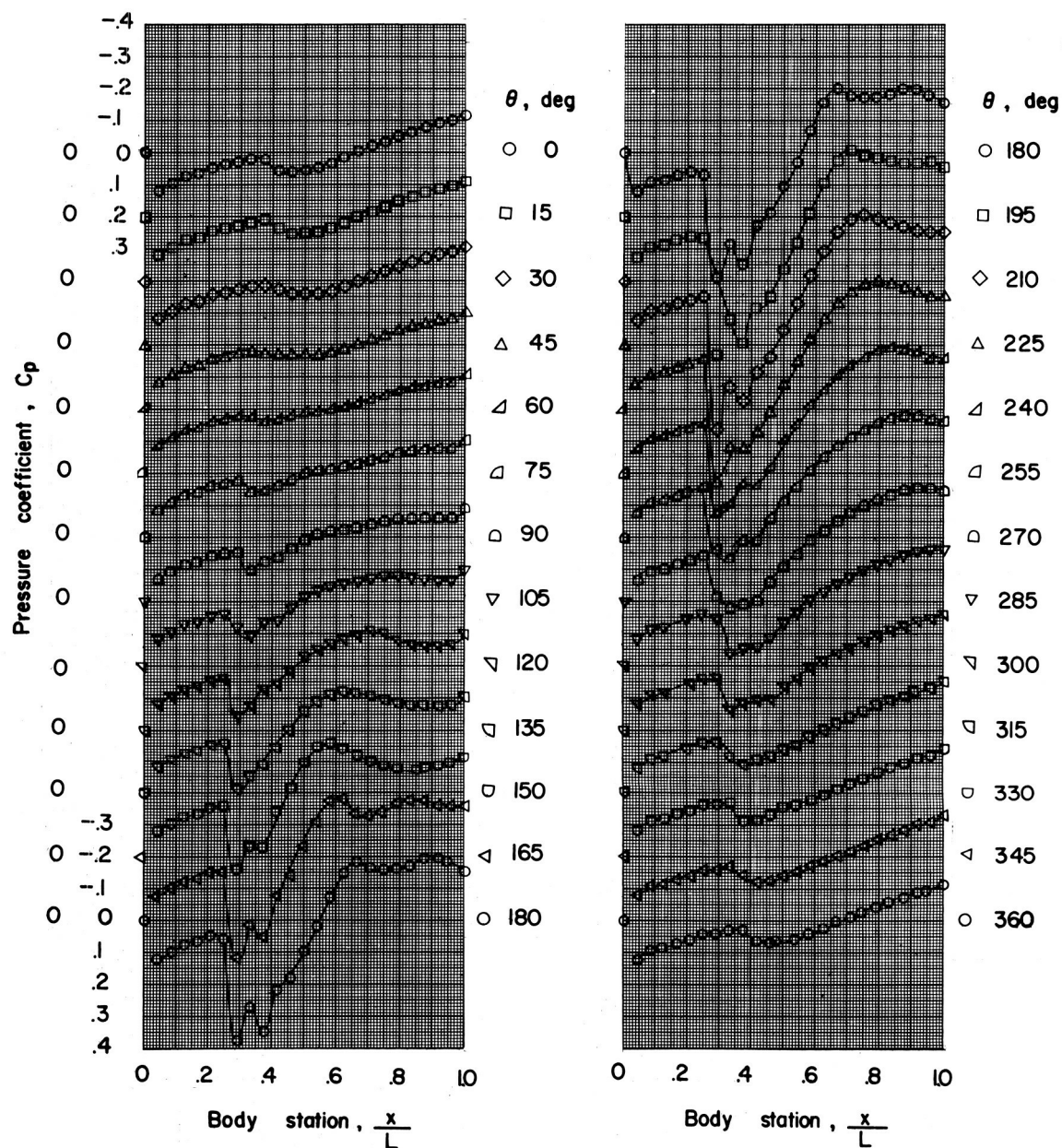
Figure 3.- Schematic layout of test grids. All dimensions are in inches.



(a)  $X = 12$ ;  $Y = 0.50$ ;  $Z = 1.50$ .

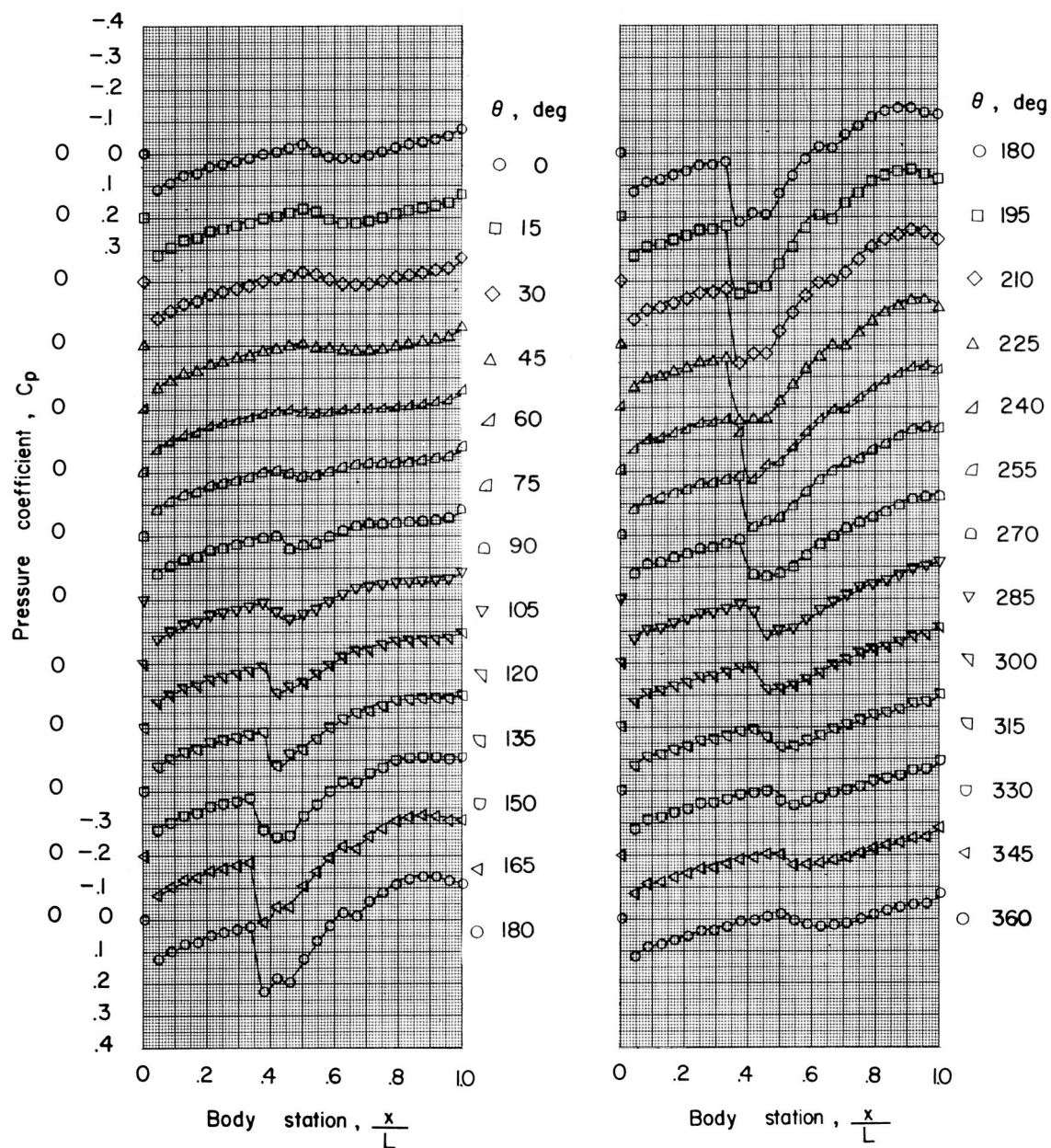
Figure 4.- Pressure-coefficient variation on the body for the various wing-body positions investigated.





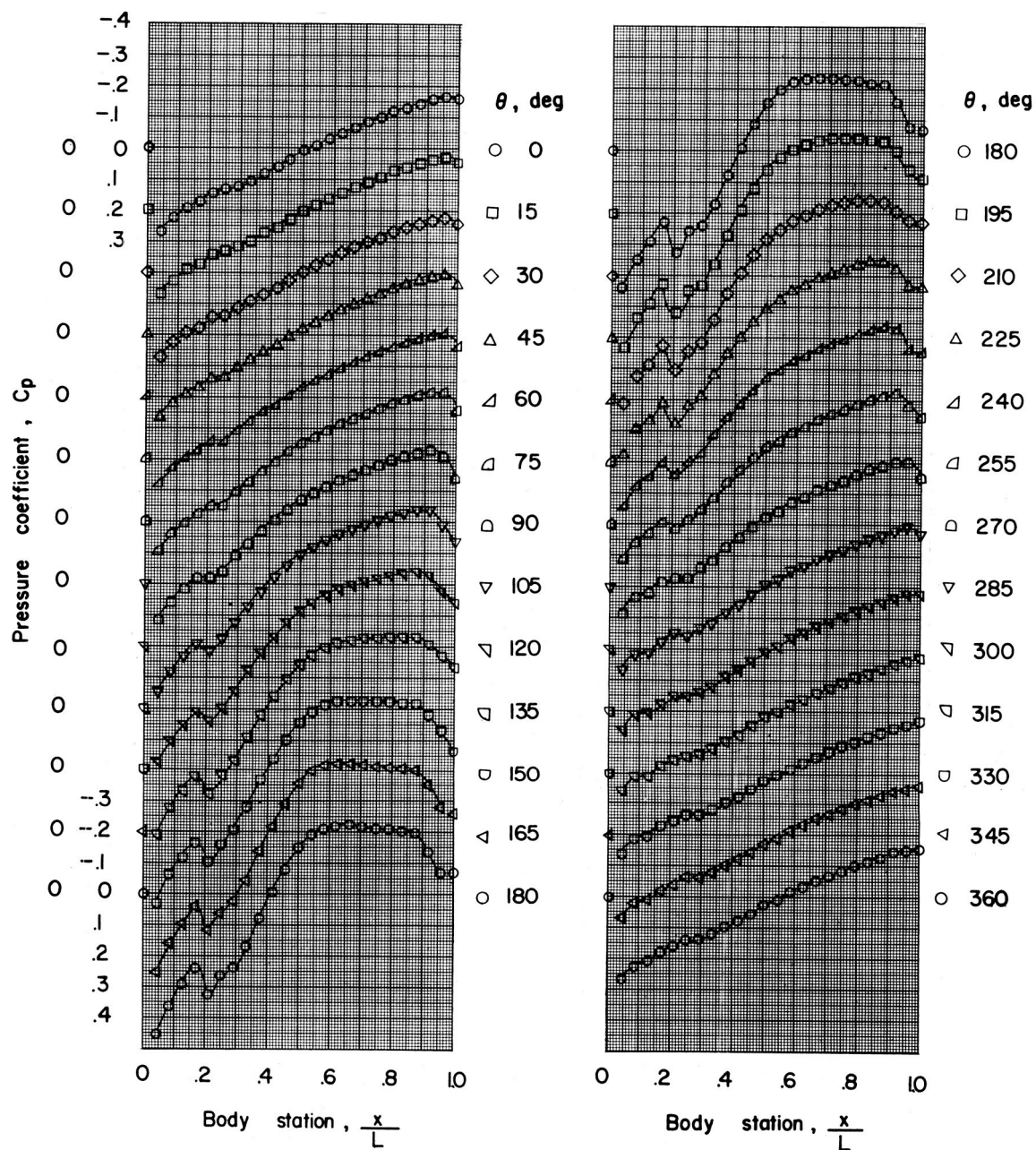
(c)  $X = 8$ ;  $Y = 0.50$ ;  $Z = 1.50$ .

Figure 4.- Continued.



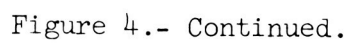
(d)  $X = 8$ ;  $Y = 0.50$ ;  $Z = 2.50$ .

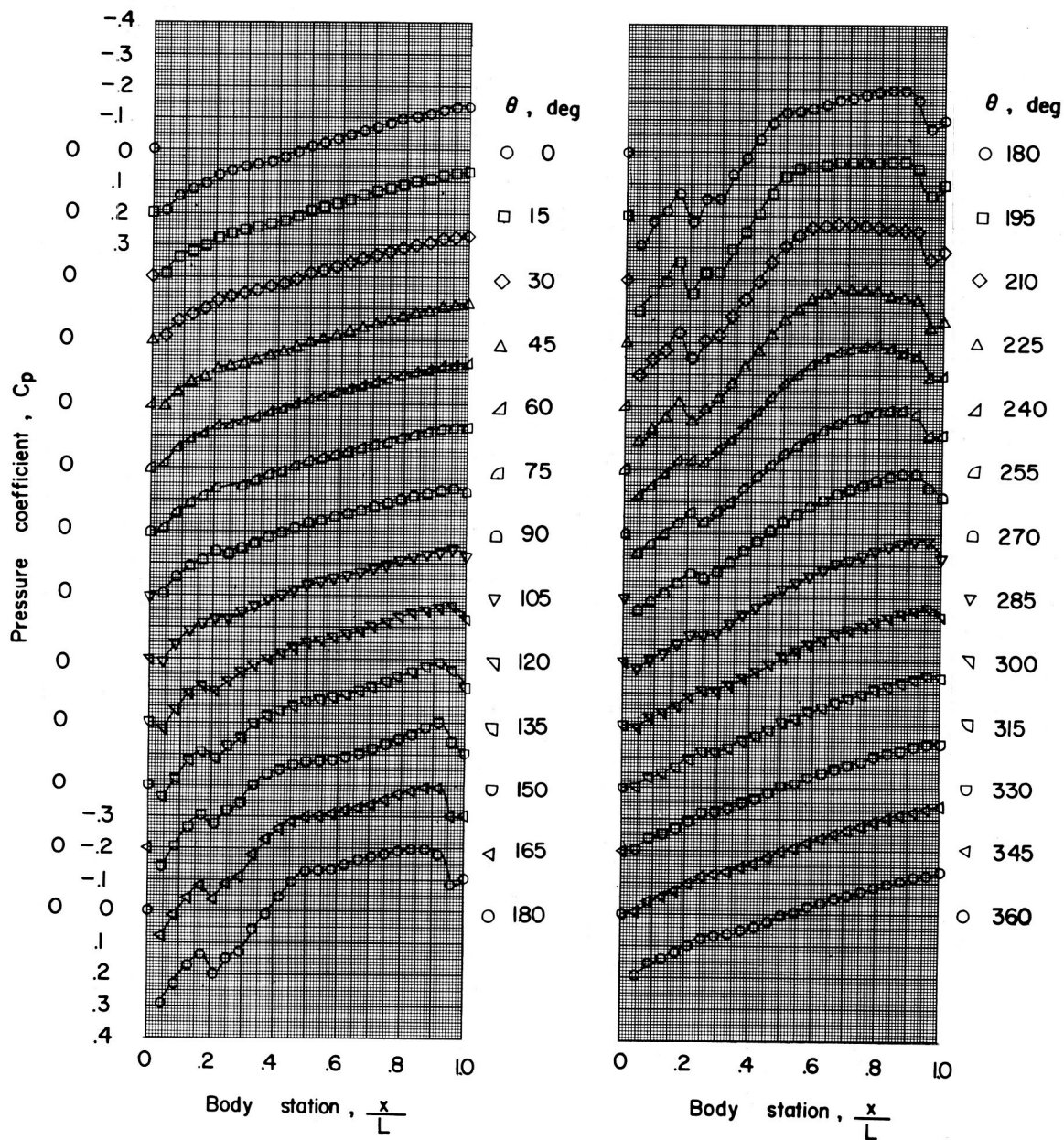
Figure 4.- Continued.



(e)  $X = 4$ ;  $Y = 4.00$ ;  $Z = 1.50$ .

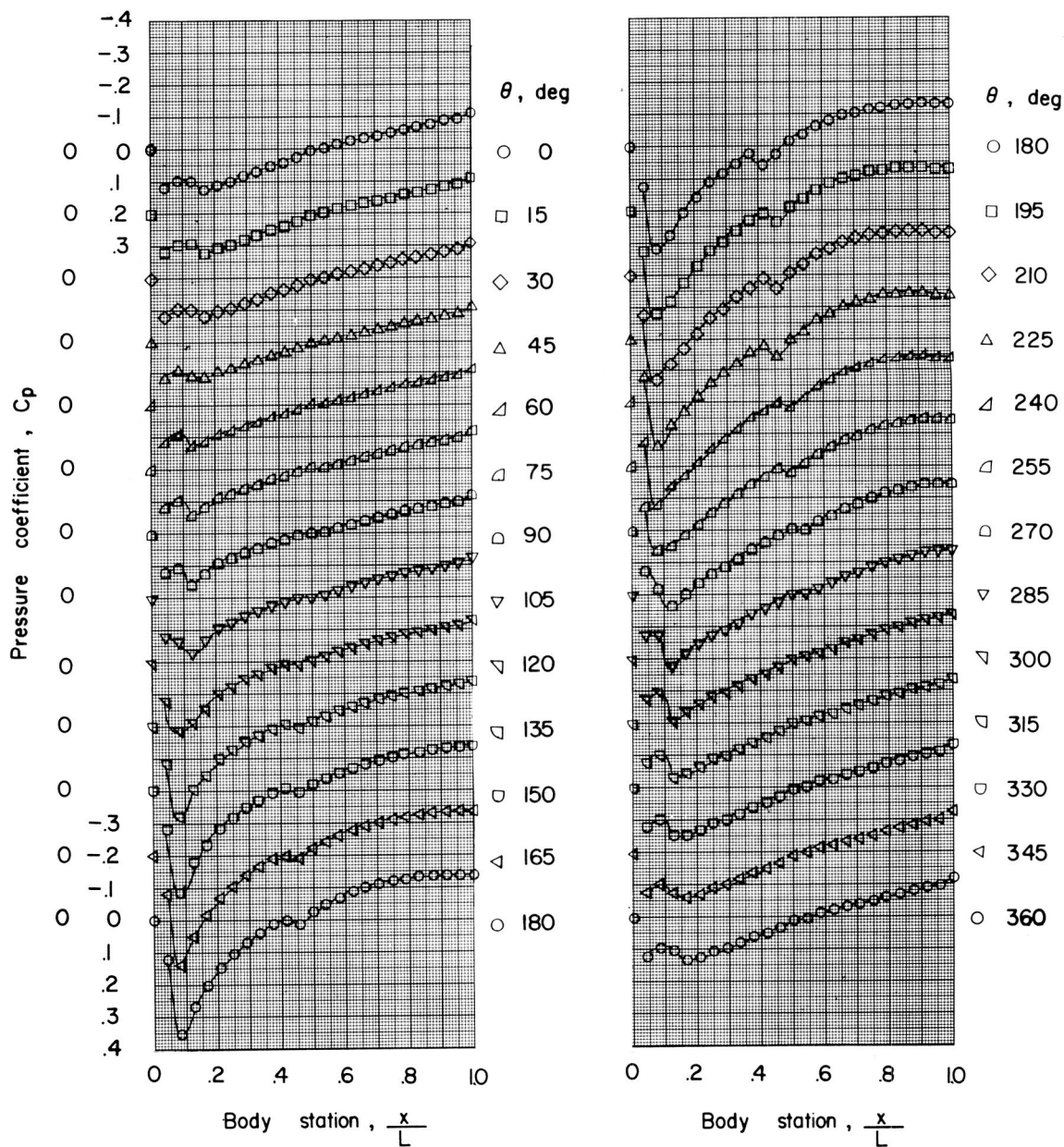
Figure 4.- Continued.





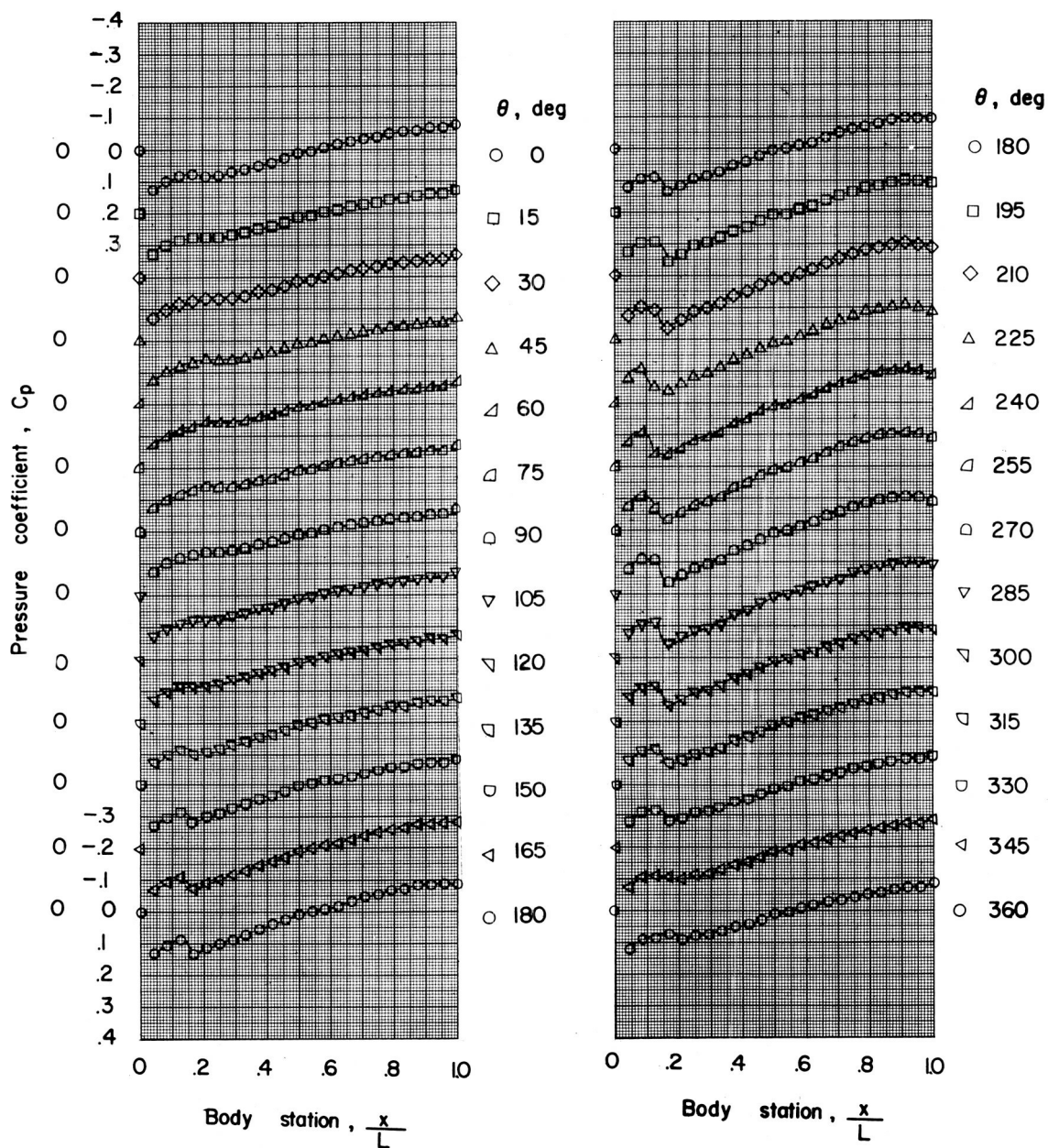
(g)  $X = 4$ ;  $Y = 0.50$ ;  $Z = 1.50$ .

Figure 4.- Continued.



(h)  $X = 4$ ;  $Y = 0.50$ ;  $Z = 2.50$ .

Figure 4.- Continued.



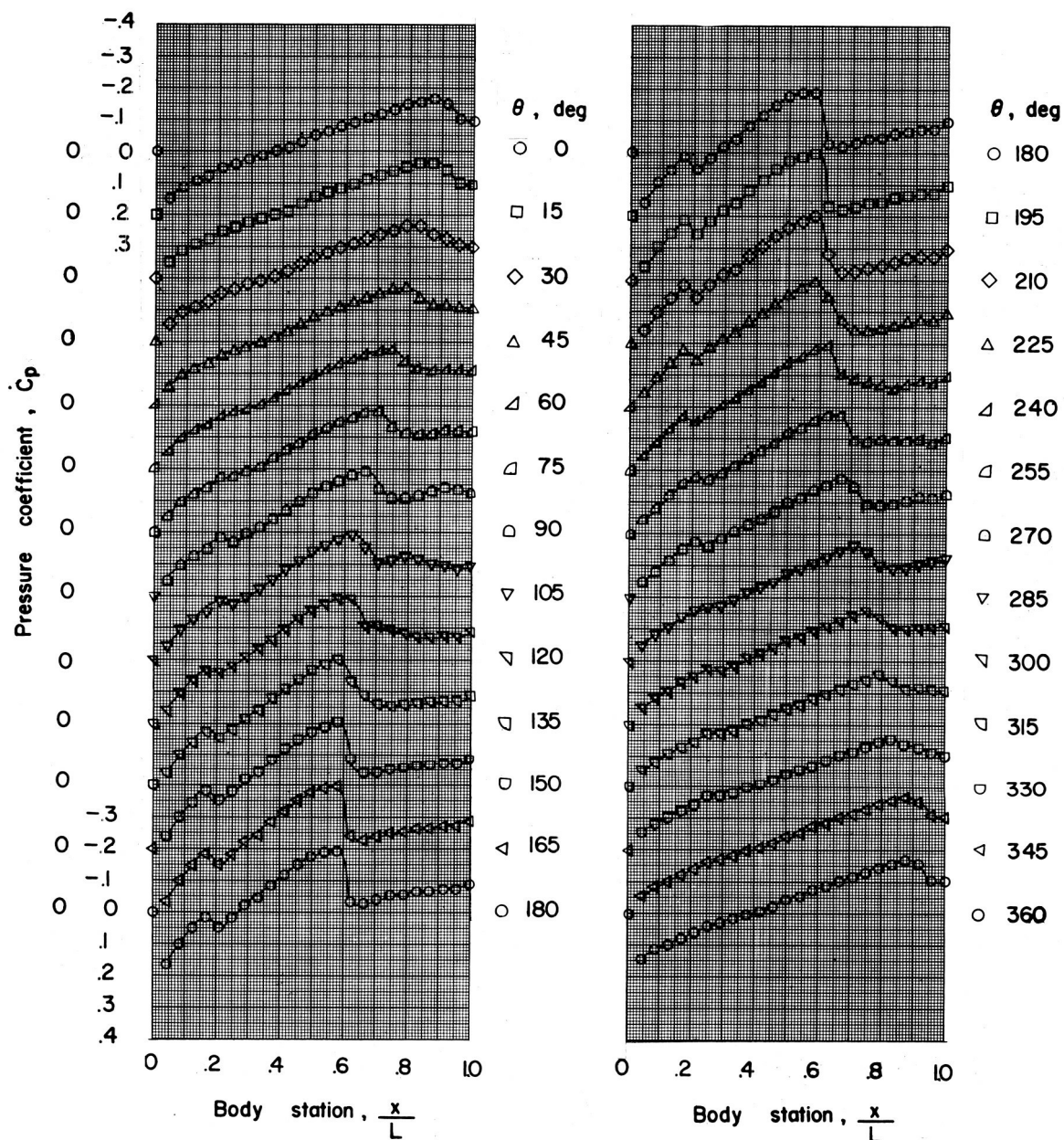
(i)  $X = 4$ ;  $Y = -1.75$ ;  $Z = 1.50$ .

Figure 4.- Continued.



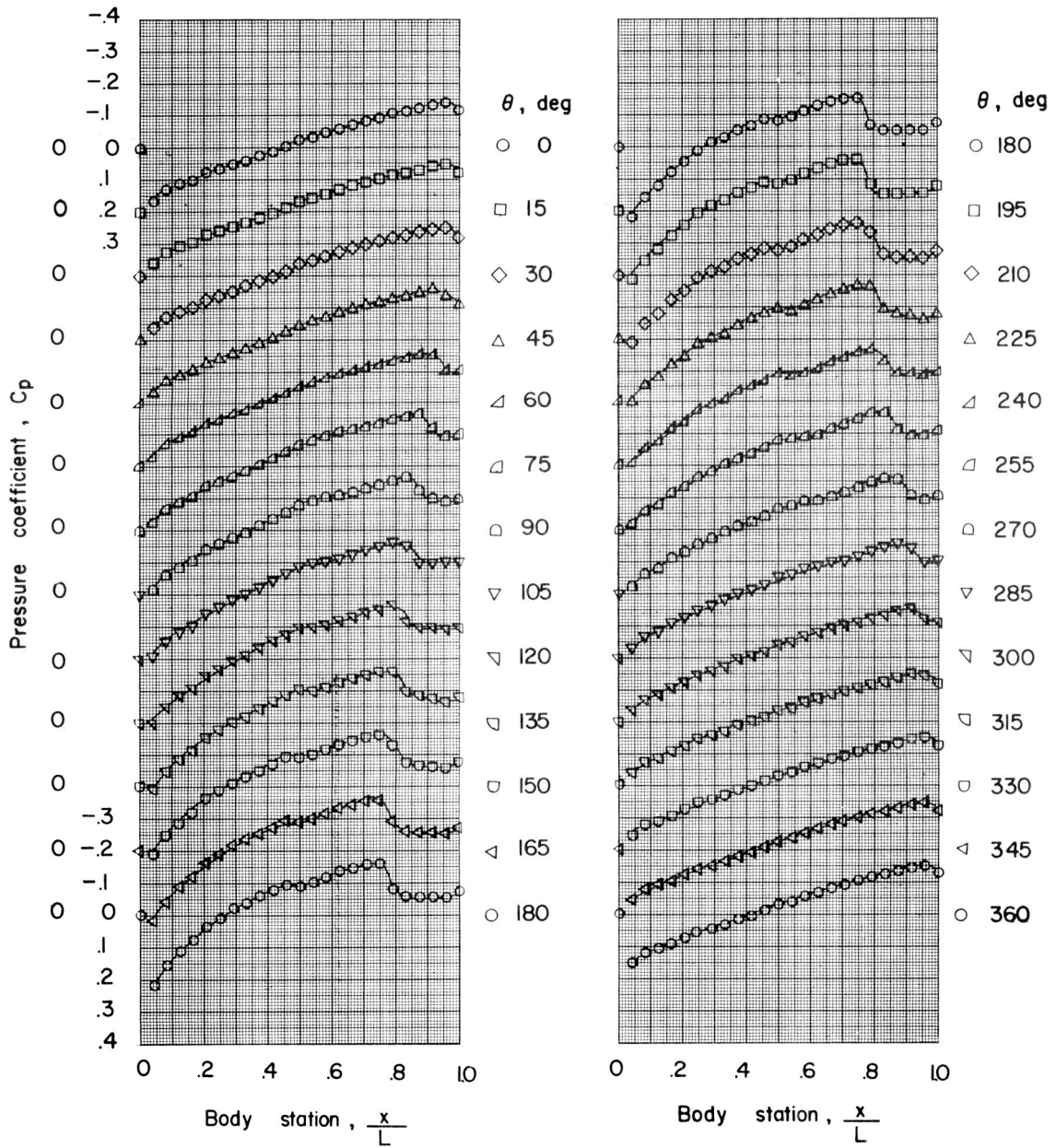
1

Figure 4.- Continued.



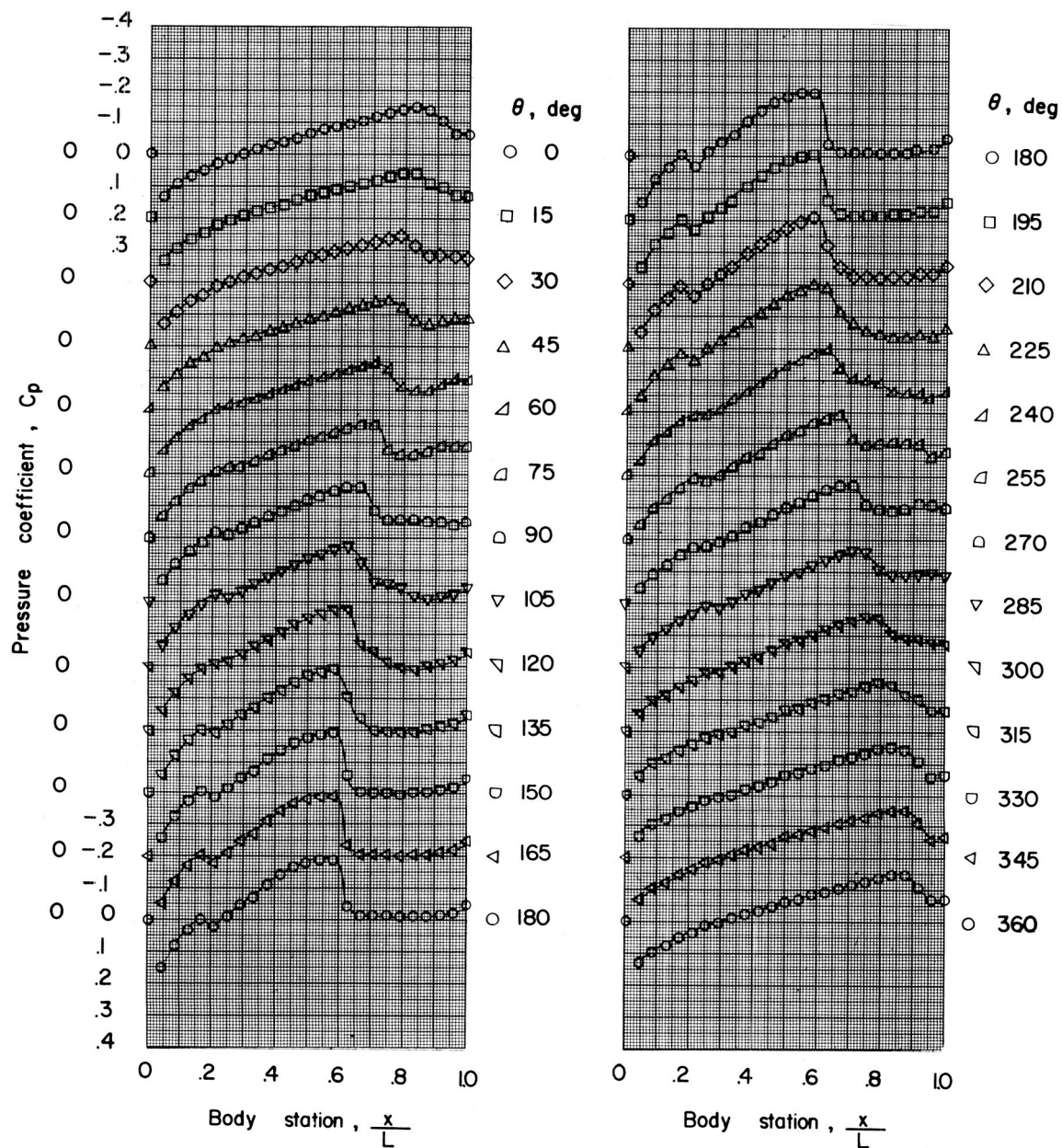
(k)  $X = 0$ ;  $Y = 7.50$ ;  $Z = 1.50$ .

Figure 4.- Continued.



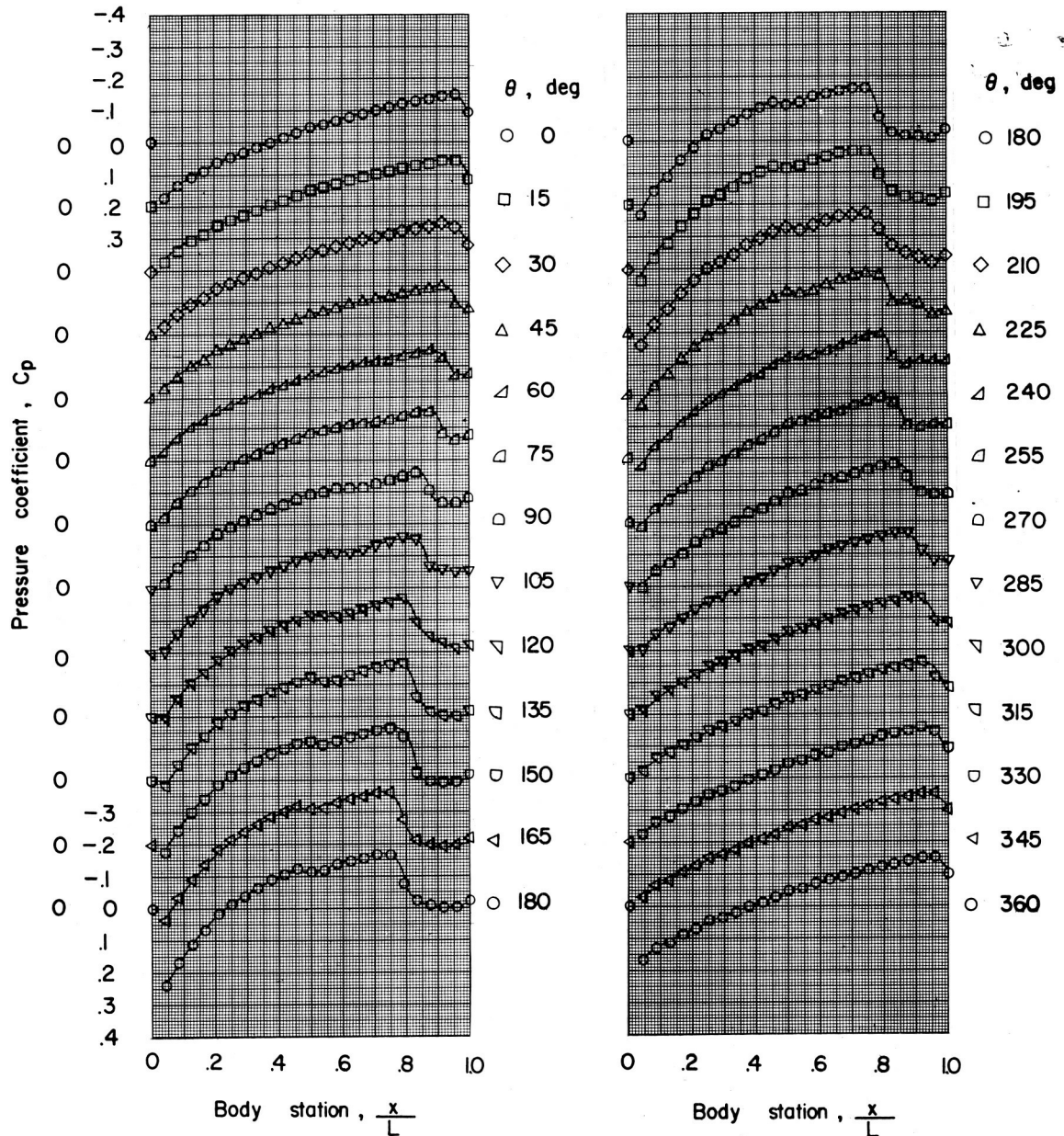
(2)  $X = 0$ ;  $Y = 7.50$ ;  $Z = 2.50$ .

Figure 4.- Continued.



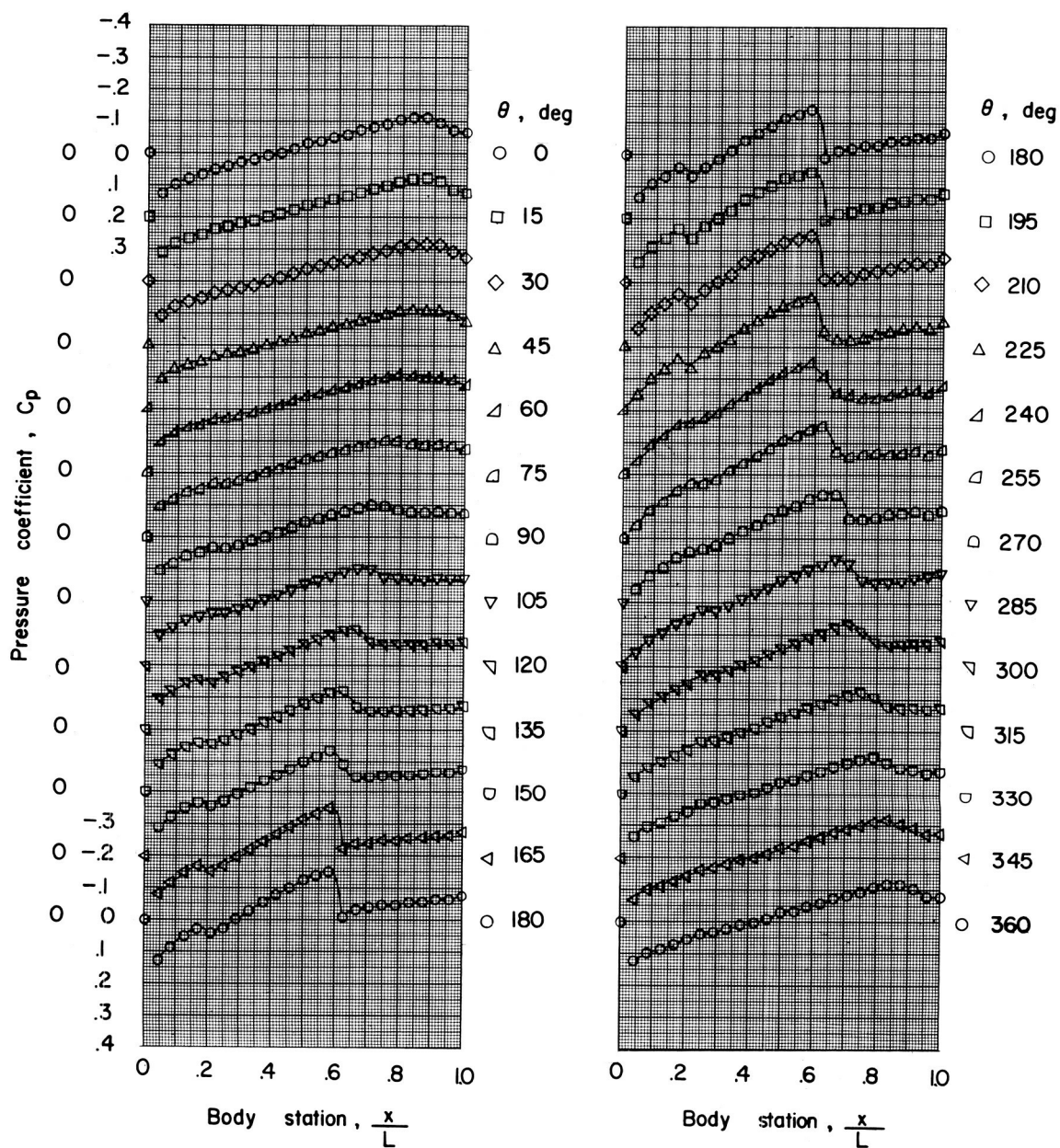
(m)  $X = 0$ ;  $Y = 4.00$ ;  $Z = 1.50$ .

Figure 4.- Continued.



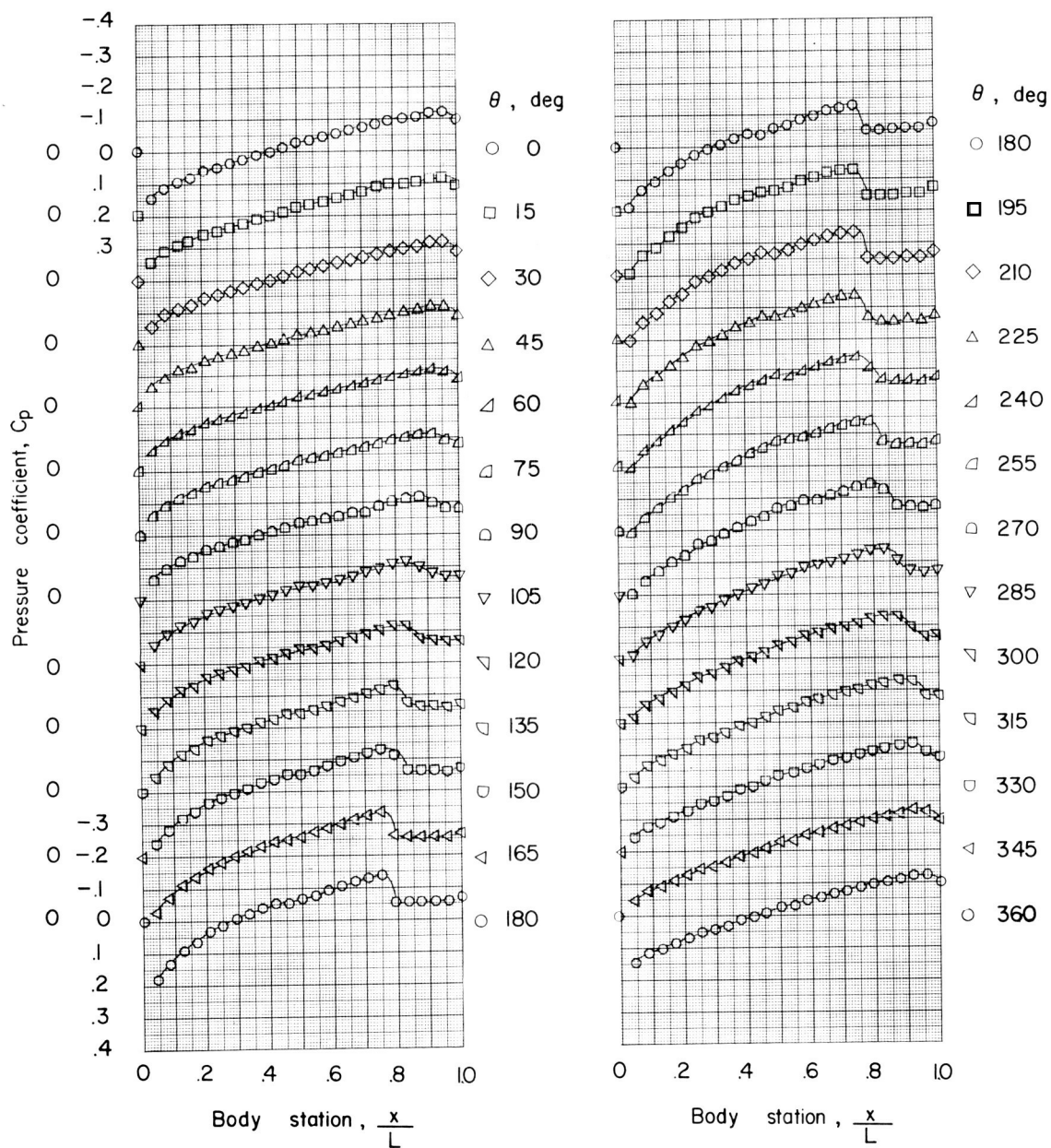
(n)  $X = 0$ ;  $Y = 4.00$ ;  $Z = 2.50$ .

Figure 4.- Continued.



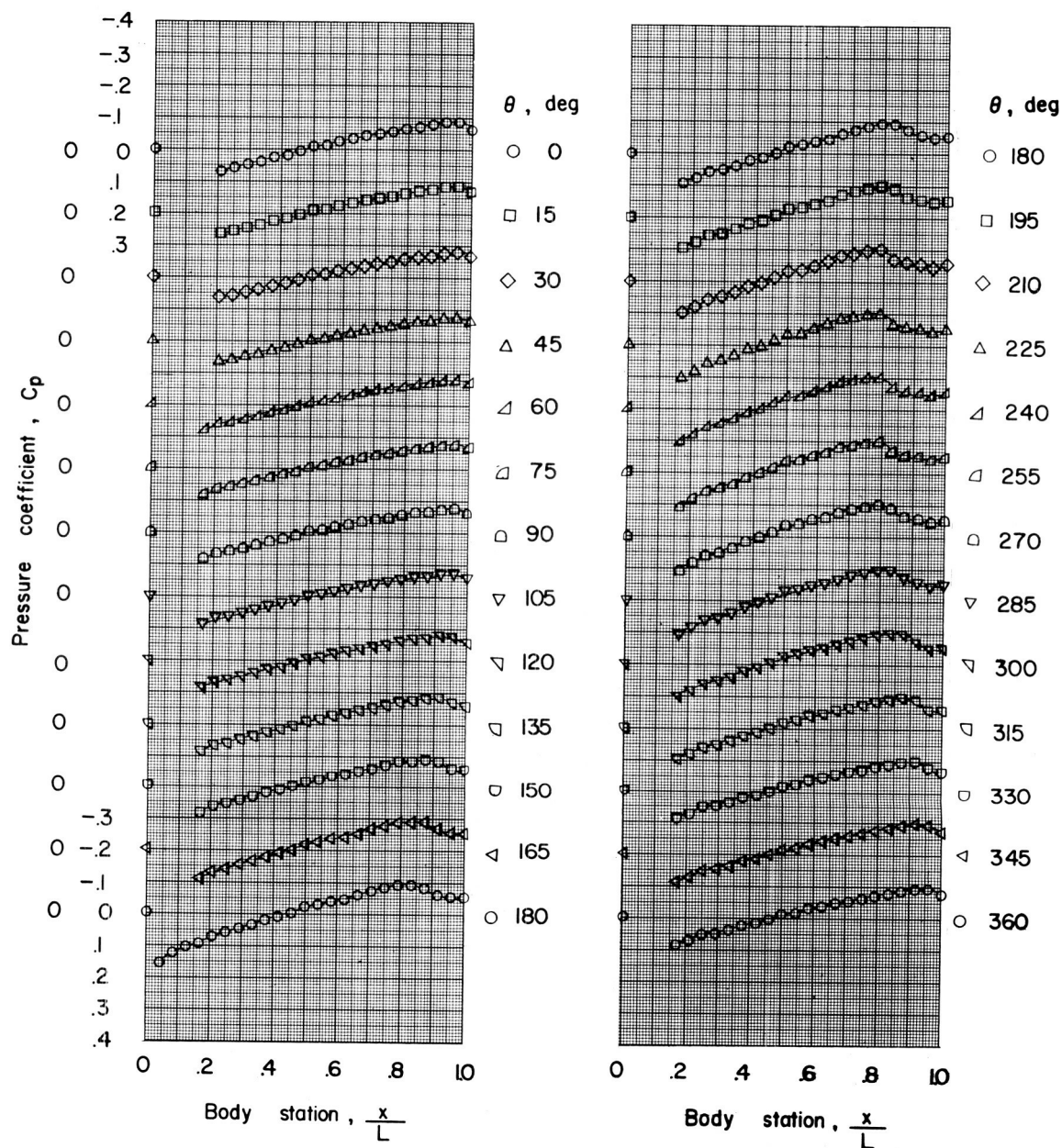
(o)  $X = 0$ ;  $Y = 0.50$ ;  $Z = 1.50$ .

Figure 4.- Continued.



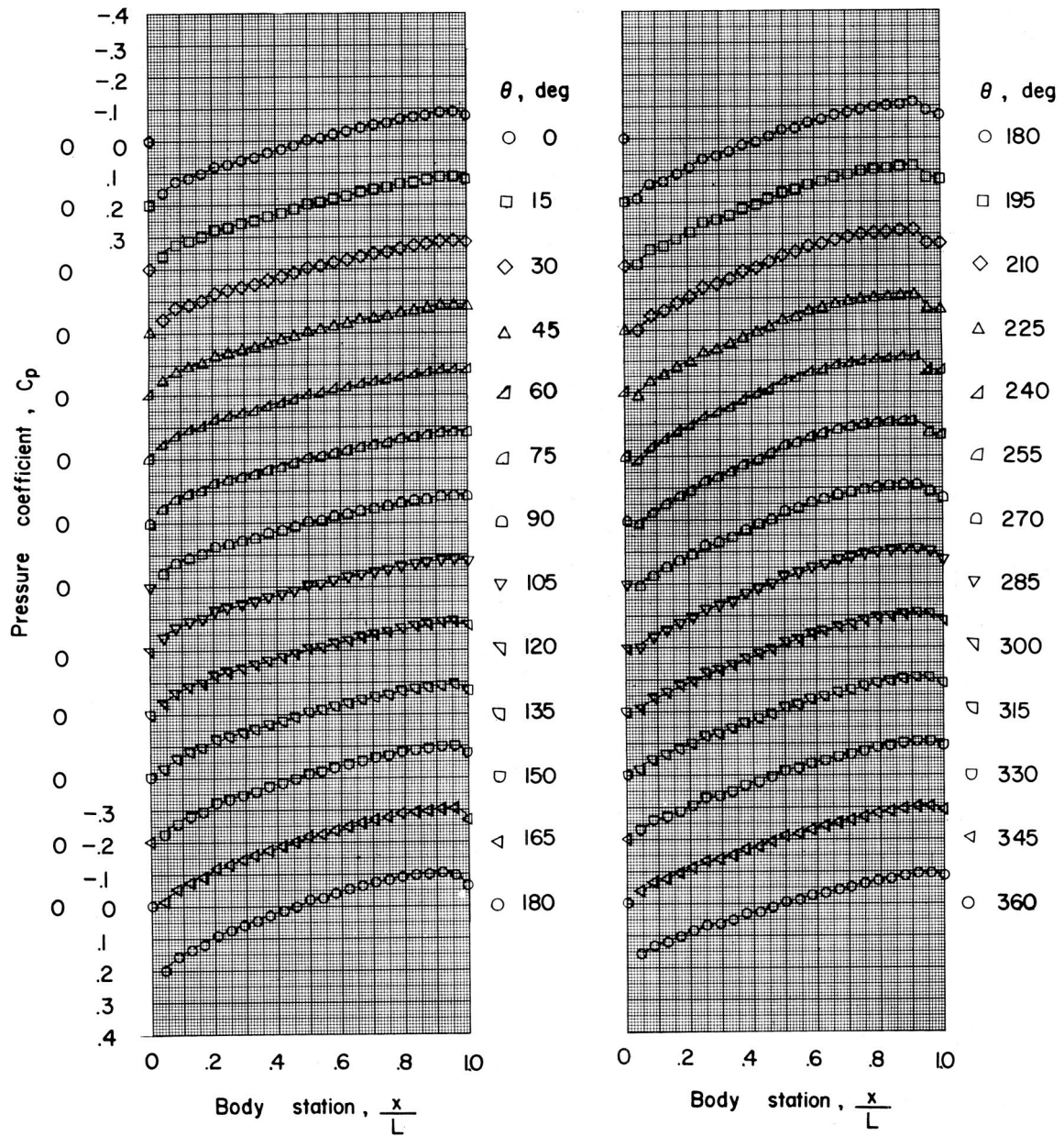
(p)  $X = 0; Y = 0.50; Z = 2.50$ .

Figure 4.- Continued.



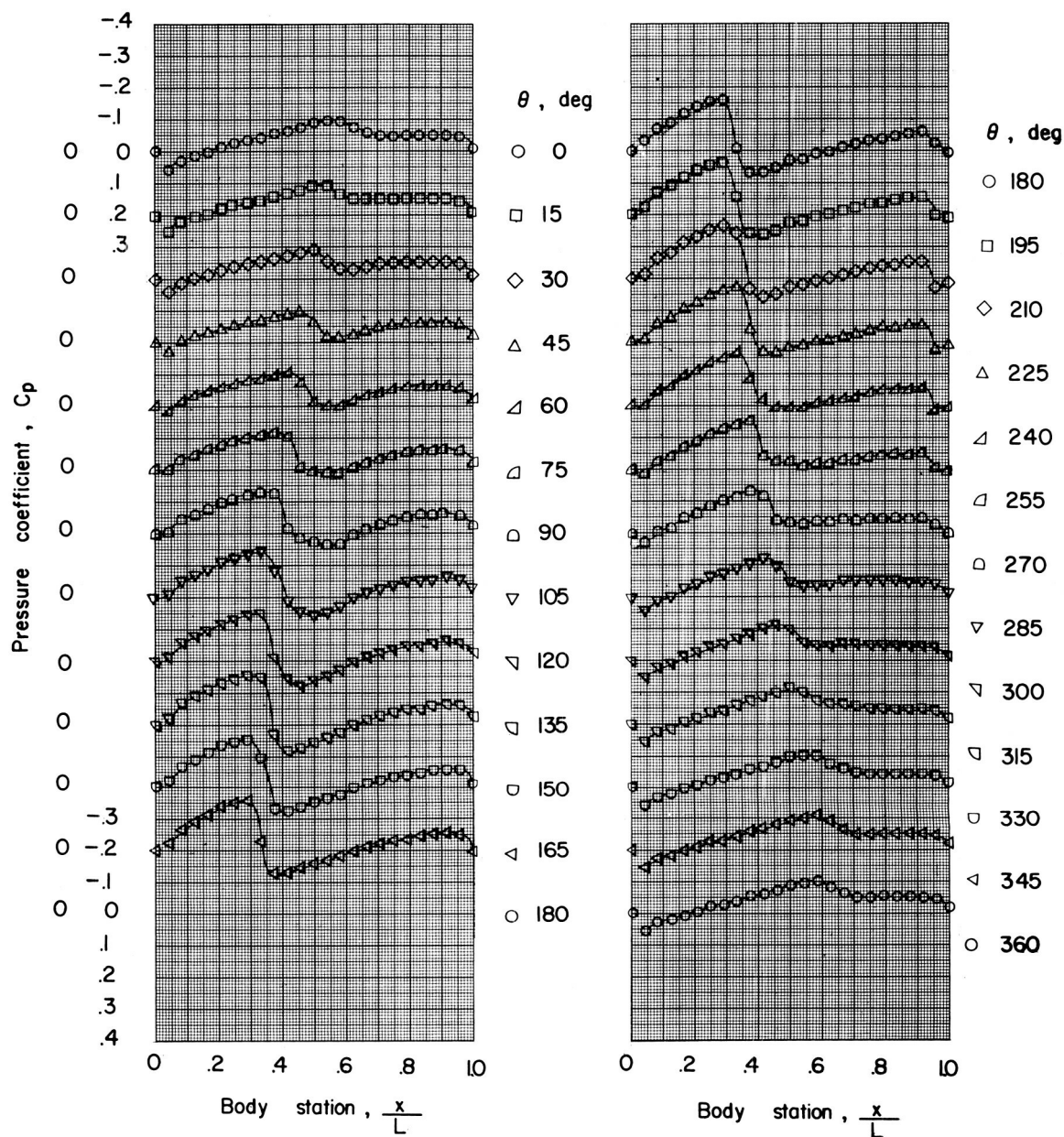
(q)  $X = 0$ ;  $Y = -1.75$ ;  $Z = 1.50$ .

Figure 4.- Continued.



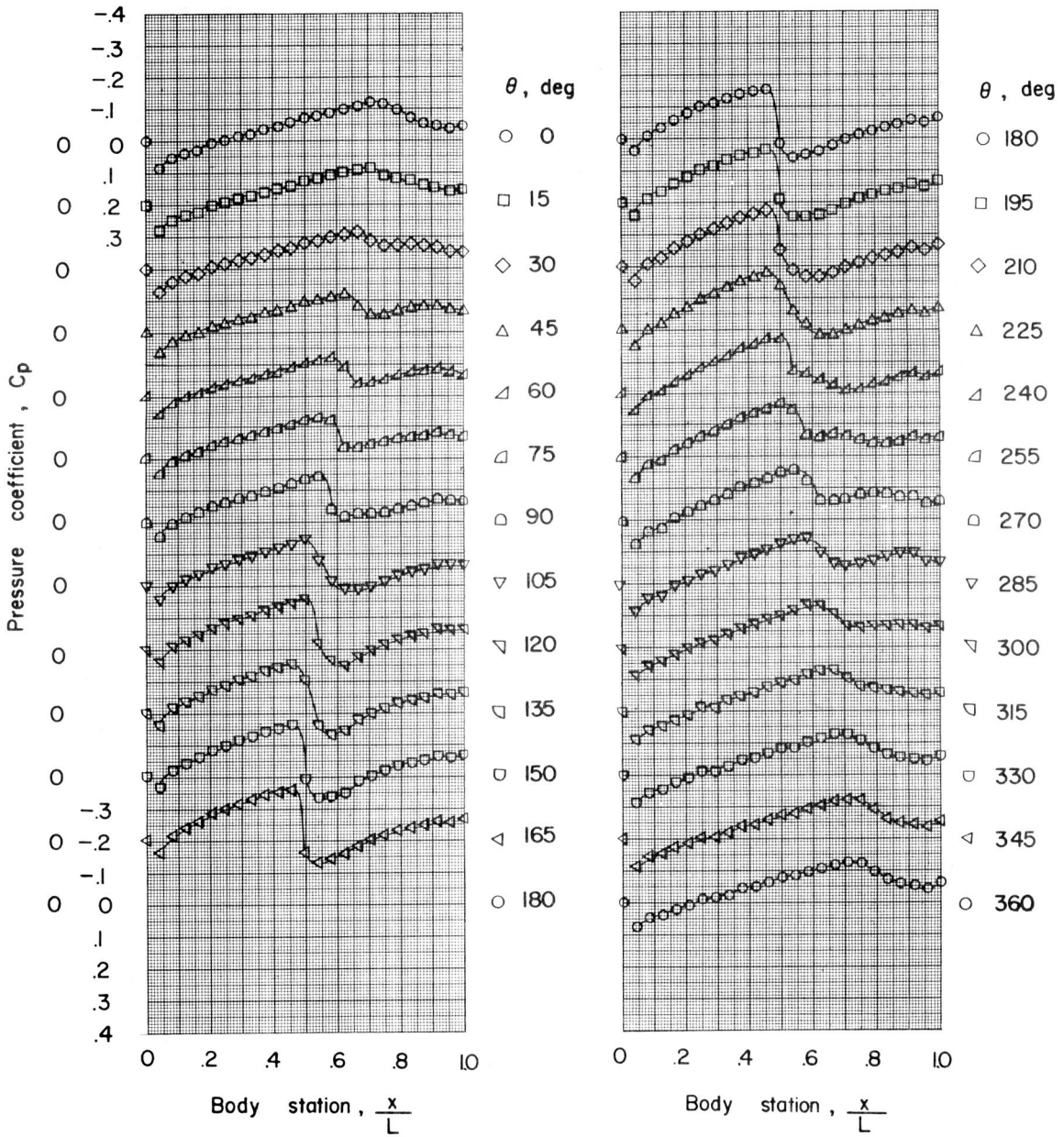
(r)  $X = 0$ ;  $Y = -1.75$ ;  $Z = 2.50$ .

Figure 4.- Continued.



(s)  $X = -4$ ;  $Y = 4.00$ ;  $Z = 1.50$ .

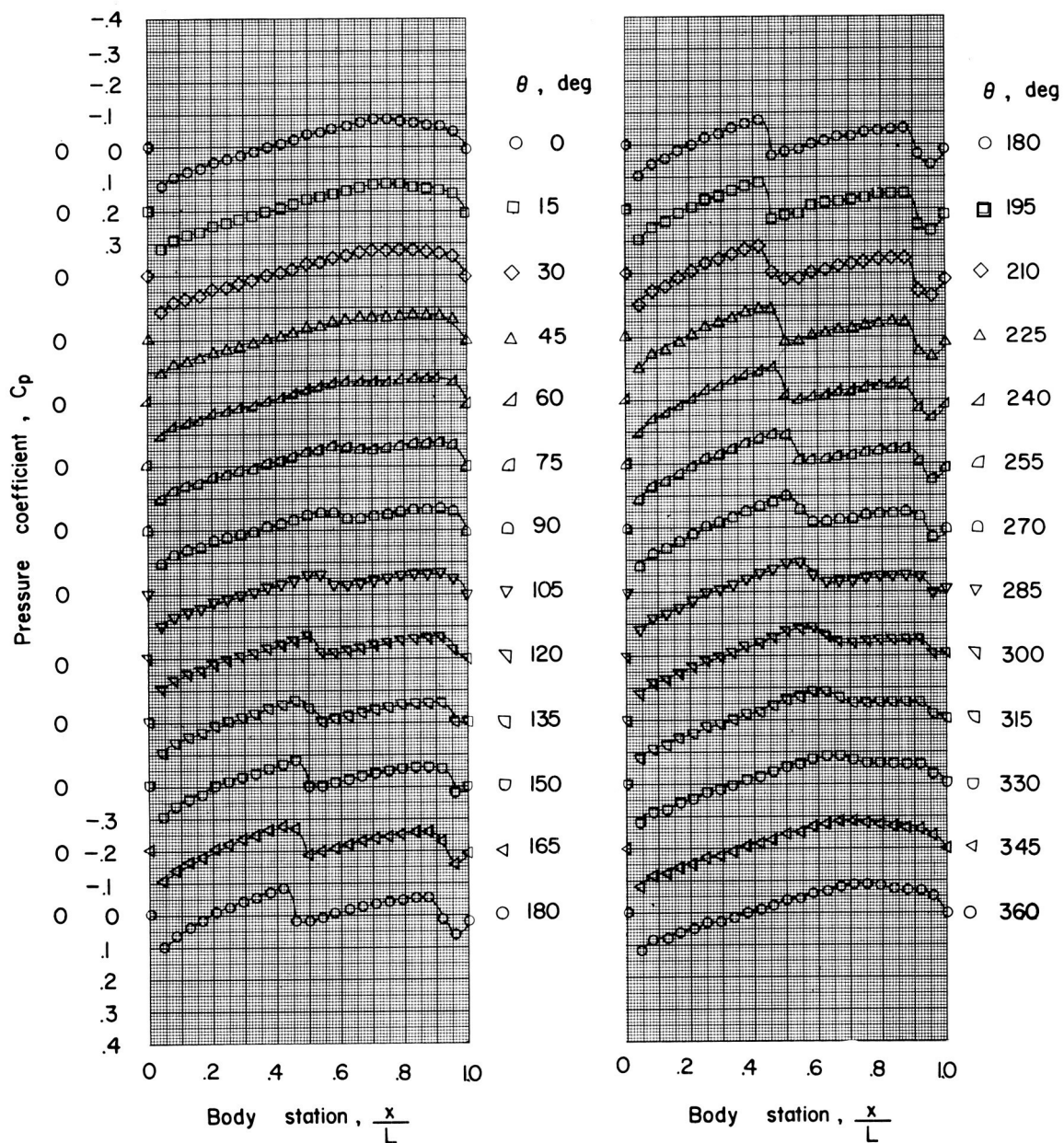
Figure 4.- Continued.



(t)  $X = -4$ ;  $Y = 4.00$ ;  $Z = 2.50$ .

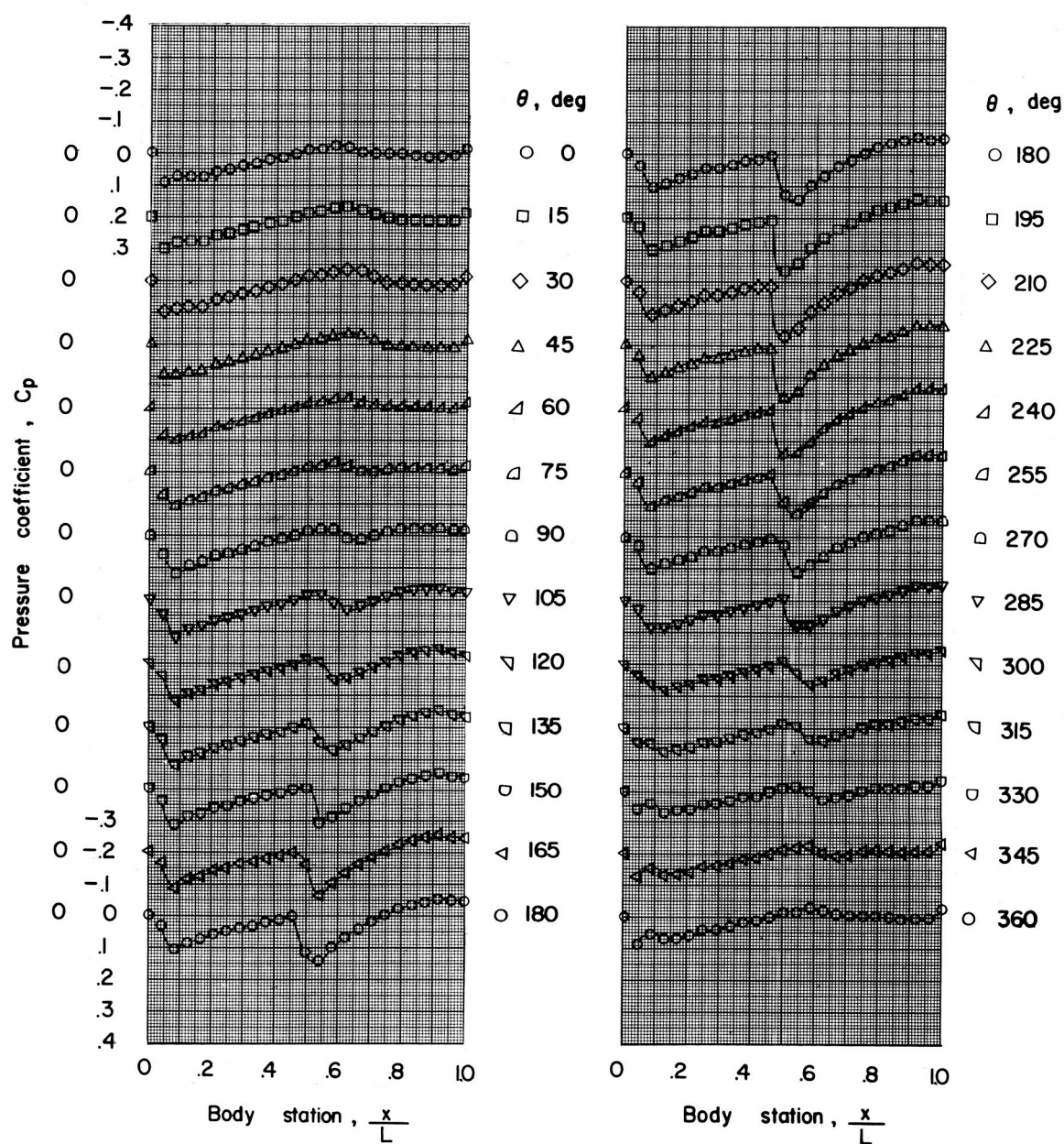
Figure 4.- Continued.





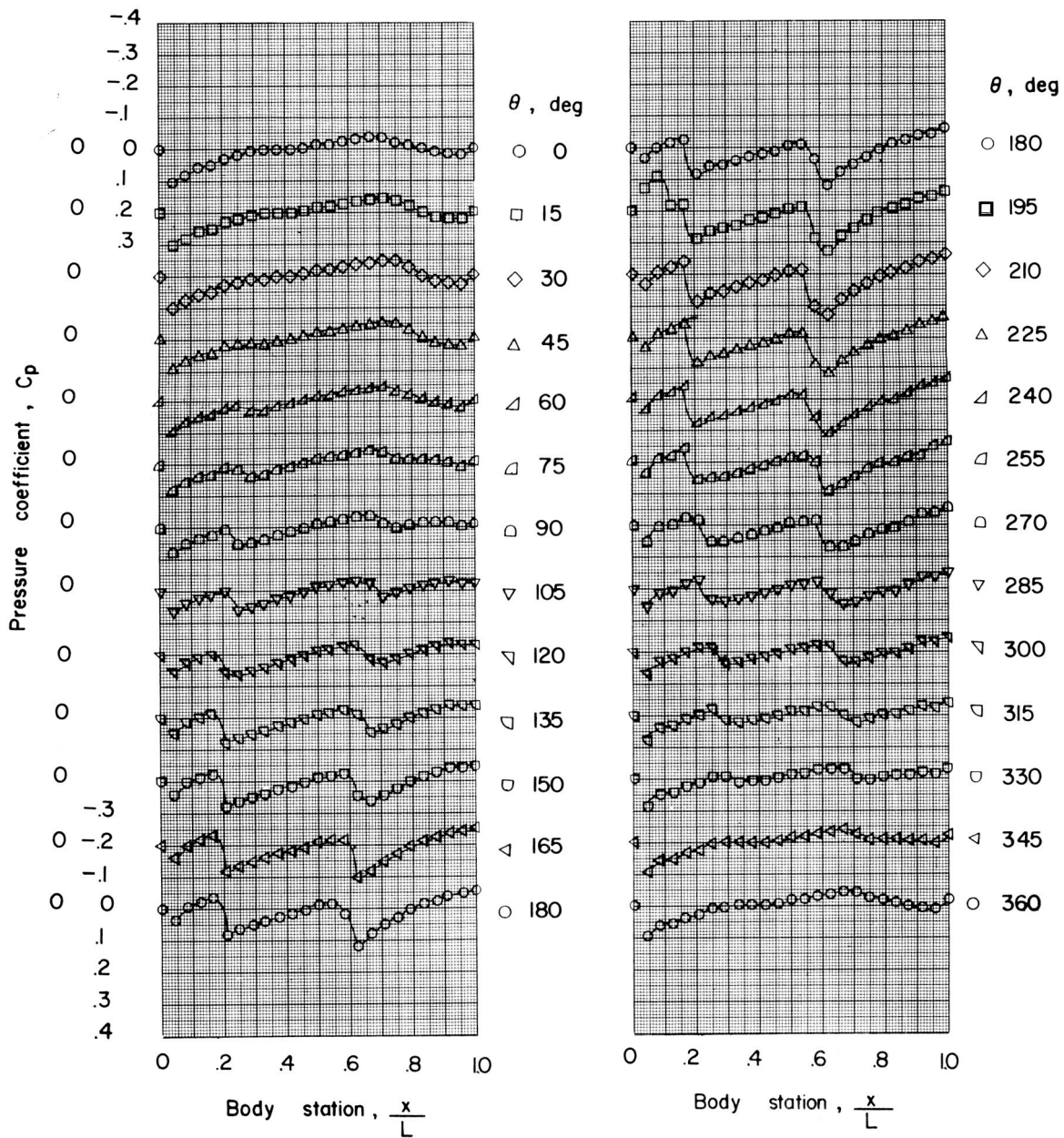
(v)  $X = -4$ ;  $Y = 0.50$ ;  $Z = 2.50$ .

Figure 4.- Continued.



(w)  $X = -8$ ;  $Y = 0.50$ ;  $Z = 1.50$ .

Figure 4.- Continued.



(x)  $X = -8$ ;  $Y = 0.50$ ;  $Z = 2.50$ .

Figure 4.- Concluded.

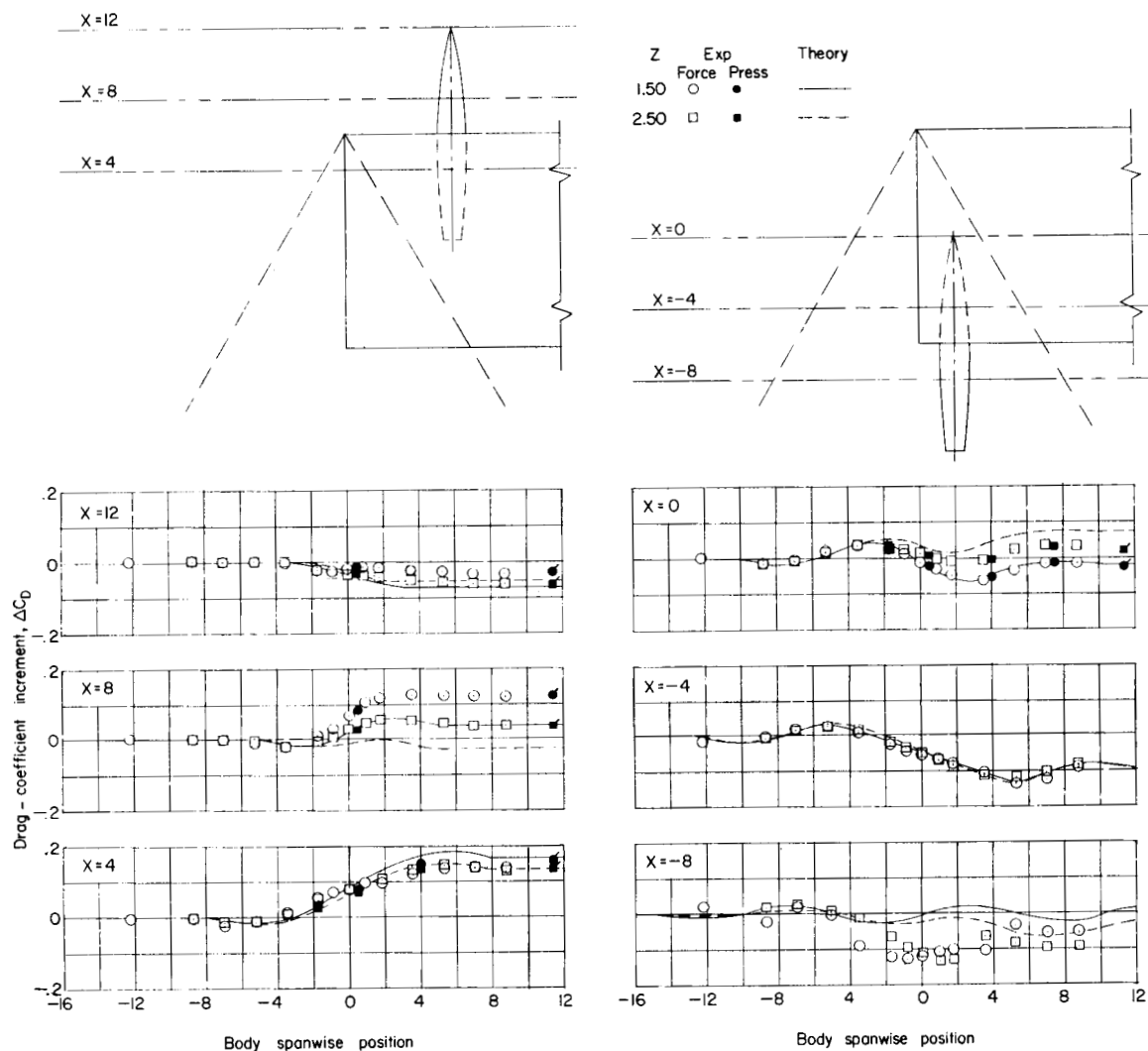


Figure 5.- Variation of the increment in body drag coefficient with wing-body position. Flagged symbols denote data from reference 2.

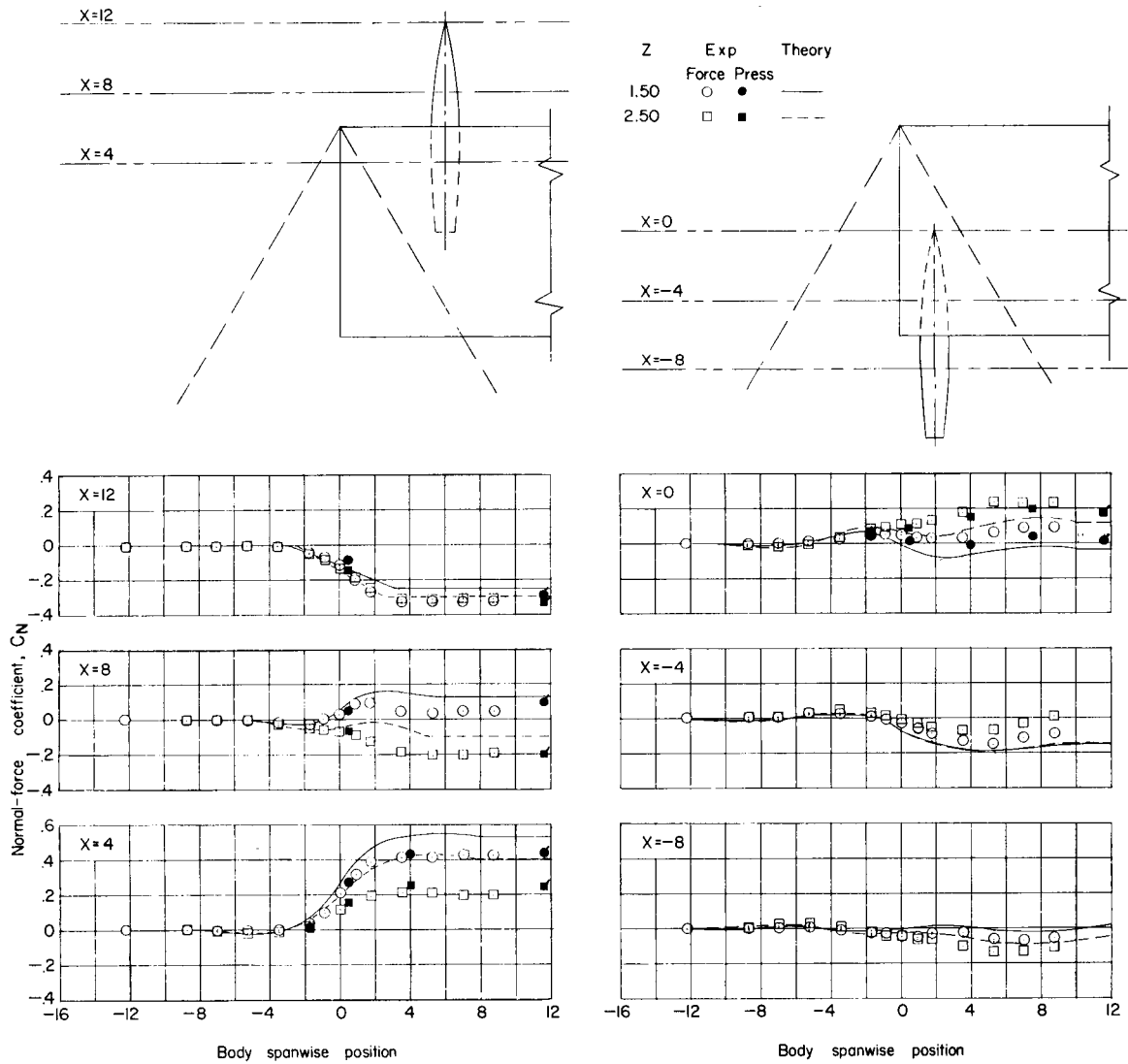


Figure 6.- Variation of the body normal-force coefficient with wing-body position. Flagged symbols denote data from reference 2.

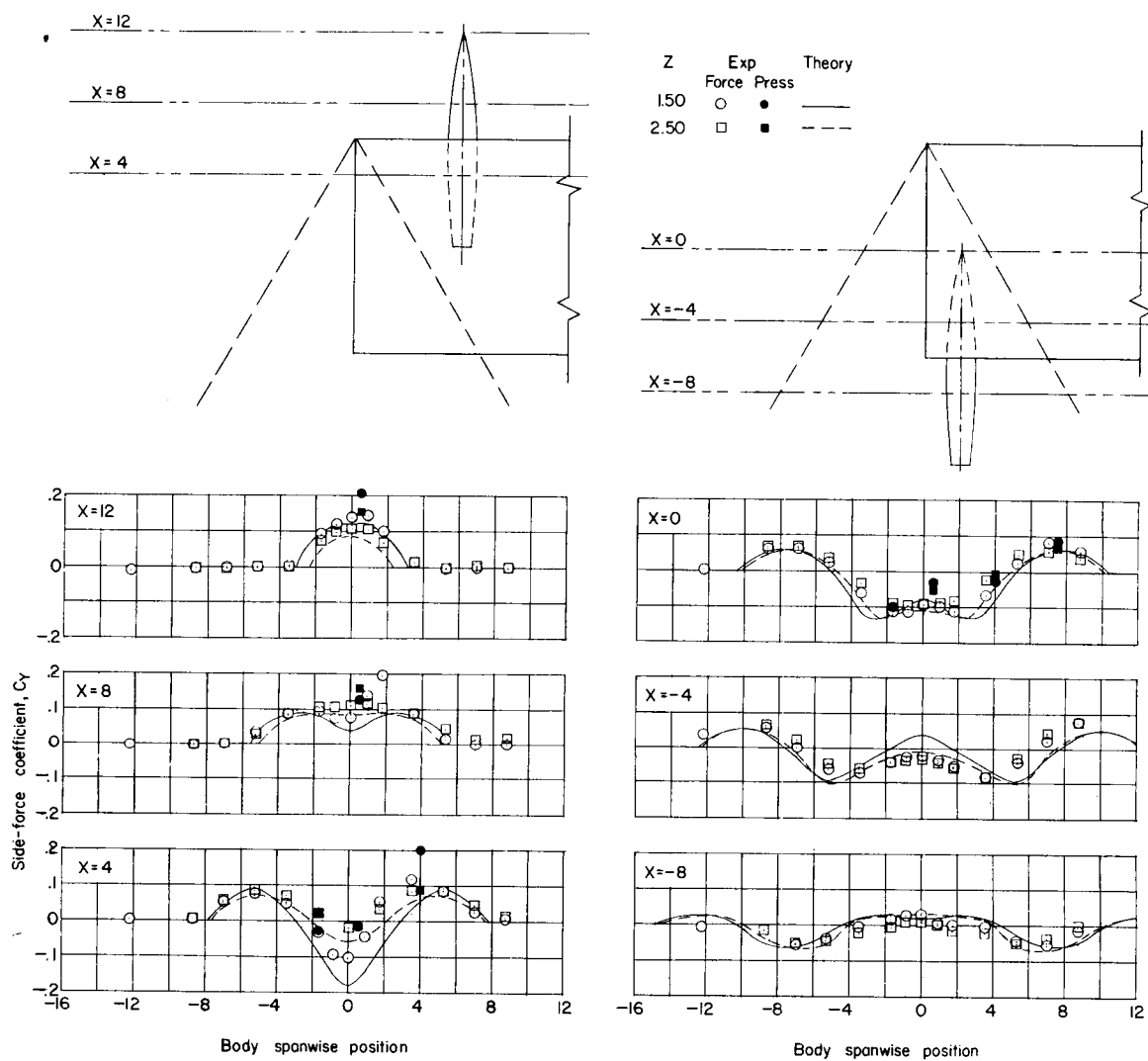


Figure 7.- Variation of the body side-force coefficient with wing-body position.

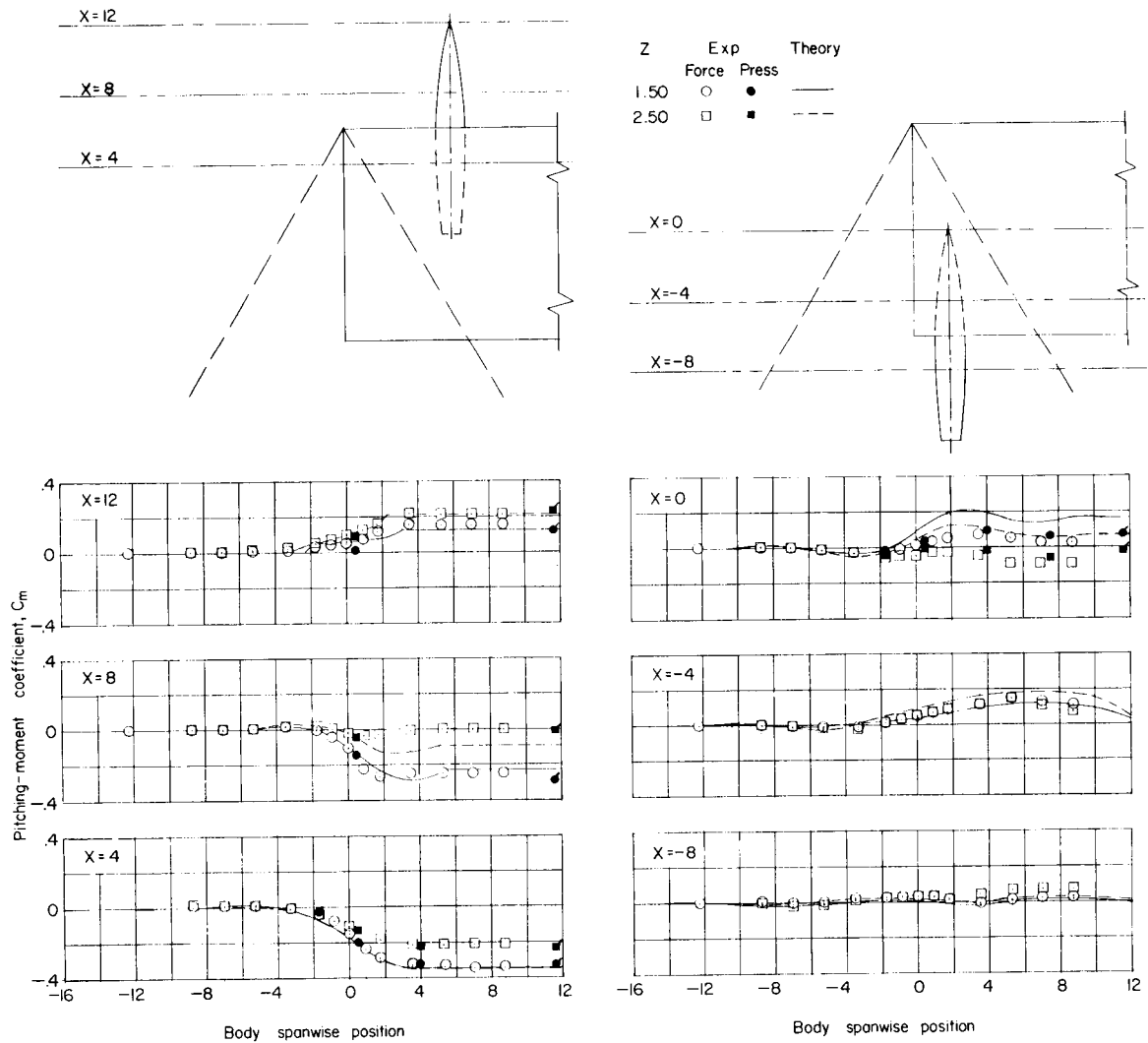


Figure 8.- Variation of body pitching-moment coefficient with wing-body position. Flagged symbols denote data from reference 2.

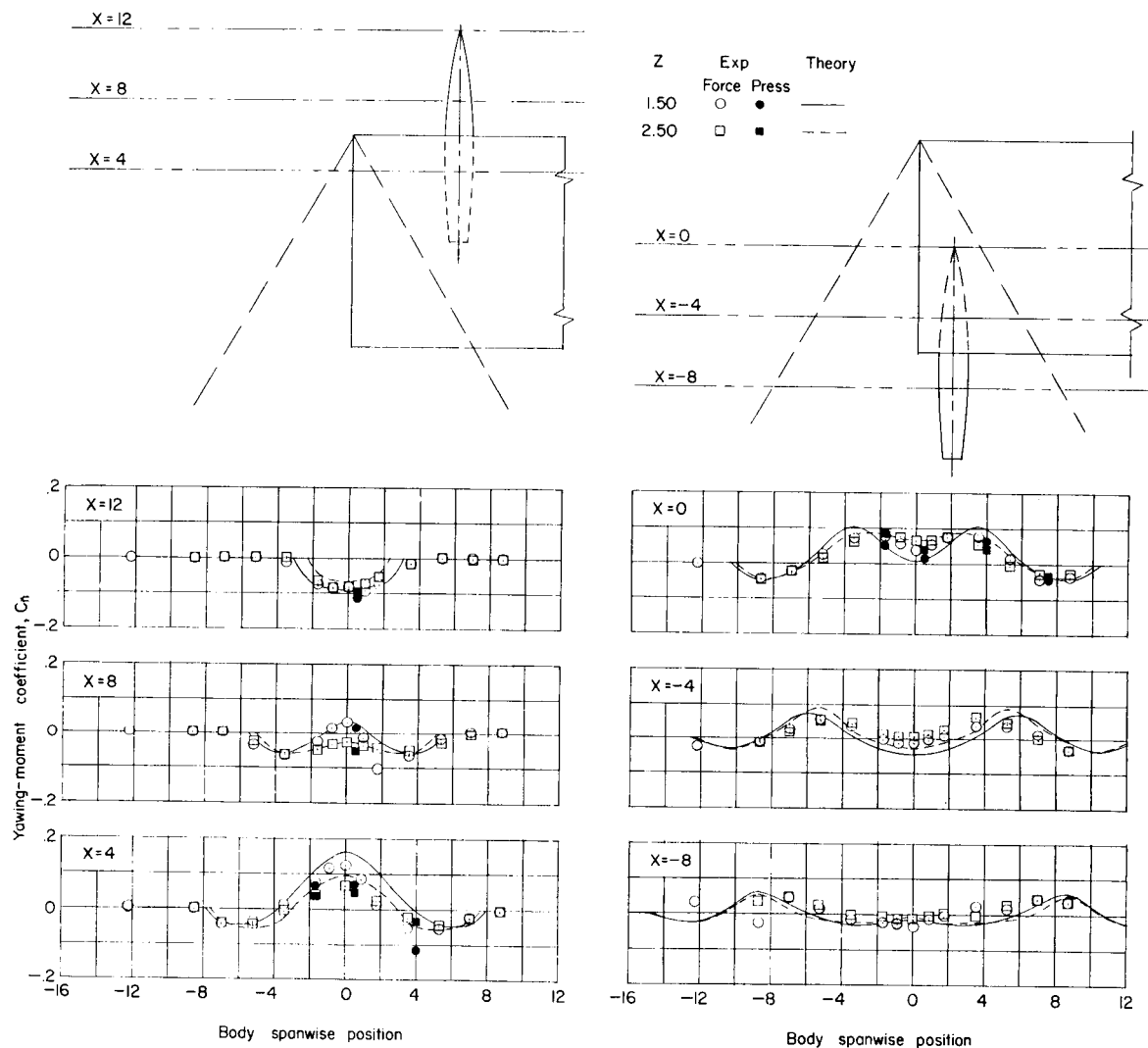


Figure 9.- Variation of body yawing-moment coefficient with wing-body position.